AGU ADVANCING EARTH AND SPACE SCIENCES

Water Resources Research

RESEARCH ARTICLE
10.1029/2025WR040349

Special Collection:
Agrohydrological Processes Under Global Change

Orchard Expansion May Diminish Groundwater Replenishment While Amplifying Nitrate Pollution in a Cultivated Loess Critical Zone

Liantao Niu[1,2], Xiaoxu Jia[1,2], Xiaofan Yang[3], Ting Yang[4], Tuvia Turkeltaub[5], Andrew Binley[6], Jan Vanderborght[7], Lidong Ren[1,2], Xiaoyong Liao[1,2], and Ming'an Shao[1,2]

[1]Modern Agricultural Engineering Laboratory, Institute of Geographic Sciences and Natural Resources Research, Chinese Academy of Sciences, Beijing, China, [2]College of Resources and Environment, University of Chinese Academy of Sciences, Beijing, China, [3]Faculty of Geographical Science, Beijing Normal University, Beijing, China, [4]Guangdong Provincial Key Laboratory of Remote Sensing and Geographical Infor-Mation System, Guangzhou Institute of Geography, Guangdong Academy of Sciences, Guangzhou, China, [5]Zuckerberg Institute for Water Research, Blaustein Institutes for Desert Research, Ben-Gurion University of the Negev, Middresht Ben Gurion, Israel, [6]Lancaster Environment Centre, Lancaster University, Lancaster, UK, [7]Agrosphere (IBG-3), Institute of Bio- and Geosciences, Forschungszentrum Jülich GmbH, Jülich, Germany

Key Points:

- Conversion of cropland to orchard reduced groundwater recharge by 10% and increased NO_3^- flux by 38 times
- Soil hydraulic heterogeneity exerts a strong control on water and NO_3^- flux, particularly in orchard systems
- NO_3^- pollution hotspots in groundwater were predicted across both cropland and orchard systems

Supporting Information:

Supporting Information may be found in the online version of this article.

Correspondence to:

X. Jia and X. Yang,
jiaxx@igsnrr.ac.cn;
xfyang@bnu.edu.cn

Citation:

Niu, L., Jia, X., Yang, X., Yang, T., Turkeltaub, T., Binley, A., et al. (2025). Orchard expansion may diminish groundwater replenishment while amplifying nitrate pollution in a cultivated loess critical zone. *Water Resources Research*, *61*, e2025WR040349. https://doi.org/10.1029/2025WR040349

Received 26 FEB 2025
Accepted 15 OCT 2025

Author Contributions:

Conceptualization: Liantao Niu, Xiaoxu Jia
Formal analysis: Liantao Niu
Funding acquisition: Xiaoxu Jia
Investigation: Xiaoxu Jia
Methodology: Liantao Niu, Xiaofan Yang, Ting Yang, Tuvia Turkeltaub, Andrew Binley
Project administration: Xiaoxu Jia
Software: Liantao Niu, Xiaofan Yang, Tuvia Turkeltaub, Andrew Binley
Supervision: Xiaoxu Jia
Validation: Liantao Niu

Abstract Agricultural land use and management changes significantly alter water and nitrate (NO_3^-) transport in the vadose zone (VZ) of the Earth's Critical Zone (CZ), thereby affecting groundwater recharge and quality. Here, we developed a multi-column modeling approach to estimate recharge and NO_3^- transport in the cultivated loess CZ of China's Guanzhong Plain (CGP), with a specific focus on the cropland-to-orchard transition. The model also quantified uncertainties in water and NO_3^- fluxes caused by variability in soil hydraulic parameters (SHPs). Evaluation against observations from 12 sites demonstrate good model performance. Relative to measured SHPs, uncertainties in groundwater recharge and NO_3^- leaching fluxes ranged from 3% to 86% when using SHPs derived from Rosetta and global data sets, with higher uncertainties in orchards than in croplands. Simulations based on measured SHPs identified the central and eastern CGP as hotpots of groundwater NO_3^- contamination. The shift from corn-wheat rotation to apple orchards increased NO_3^- leaching fluxes by 38 times while reducing groundwater recharge by 10%. Under both land-use scenarios, NO_3^- travel times through the VZ spanned decades to centuries, and the cropland-to-orchard transition extended it by 23 years for NO_3^- to reach the aquifer. Although this conversion delays NO_3^- transport to the aquifer, the elevated leaching flux increases the risk of groundwater NO_3^- pollution, especially in regions with shallow VZs and coarse soil texture. This study highlights the critical need for caution when implementing large-scale cropland-to-orchard conversions in the CGP and provides important insights for groundwater vulnerability assessments in regions with comparable hydrogeological and agricultural conditions.

Plain Language Summary Agricultural land-use and management changes significantly alter vadose zone hydrology and nitrate (NO_3^-) transport within the Earth's Critical Zone (CZ). In this study, we built a model that uses many vertical soil columns to represent the soil. We used this model to estimate how much water reaches the groundwater and how much NO_3^- moves downward under two land use systems: traditional cropland and orchards. We also tested how differences in soil hydraulic properties affect the results. These differences create large uncertainties in the predicted amount of water recharge and NO_3^- leakage, especially in orchards. In the central and eastern parts of the region, groundwater is more susceptible to NO_3^- pollution. Converting cropland to orchards reduces the amount of water reaching the groundwater but increases the amount of NO_3^- moving downward, raising the risk of groundwater pollution. Future large-scale shifts from croplands to orchards require caution, particularly in regions with shallow soil and coarse texture.

1. Introduction

Groundwater nitrate (NO_3^-) contamination represents a significant environmental challenge worldwide, especially in regions with intensive agricultural practices and high nitrogen (N) fertilizer applications (Xue et al., 2009; Zhu et al., 2023). Studies have shown that NO_3^- tends to accumulates in the vadose zone (VZ), particularly in areas with thick VZs and long histories of agricultural activity, as observed across parts of China,

Visualization: Liantao Niu
Writing – original draft: Liantao Niu
Writing – review & editing: Xiaoxu Jia, Xiaofan Yang, Ting Yang, Tuvia Turkeltaub, Andrew Binley, Jan Vanderborght, Lidong Ren, Xiaoyong Liao, Ming'an Shao

North America, and Europe (Ascott et al., 2017; Yang, Wu, Dong, et al., 2020). This accumulation poses substantial risks to subsurface environments due to NO_3^-'s high water solubility, limited uptake by plant roots in the deep VZ, and weakened denitrification processes (Mahvi et al., 2005; Rao & Puttanna, 2000; Wang et al., 2019; Wang, X et al., 2015; Zhang et al., 2013). Understanding NO_3^- transport patterns within the VZ helps to determine the quantity and timing of NO_3^- reaching groundwater, thereby facilitating the assessment of groundwater NO_3^- contamination risks.

NO_3^- transport in the VZ is shaped by several factors, including soil properties, land-use types, and agricultural management practices (Bohlke, 2002; Green et al., 2008; Liao et al., 2012; Robertson et al., 2017). Soil properties, such as texture, porosity, and organic matter content, exert a strong control on NO_3^- transport through the soil matrix (Fatichi et al., 2020; Wang et al., 2019). Different land-use types (e.g., croplands, orchards, natural vegetation) exhibit distinct NO_3^- transport behaviors, driven by differences in water consumption, root distribution depth, and nutrient cycling processes (Padilla et al., 2018; Turkeltaub et al., 2015, 2021). Additionally, agricultural management, such as tillage, irrigation, fertilization, and drainage systems, can significantly alter soil hydrological regimes and nutrient dynamics, thereby reshaping NO_3^- transport pathways in the VZ (Bowles et al., 2018; Gao et al., 2019; Suchy et al., 2018; Wang et al., 2023). Recent studies in intensively agricultural regions of China have revealed that the conversion of croplands to orchards often leads to substantial NO_3^- accumulation in the deep VZ (Yang, Wu, Song, et al., 2020; Gao, J et al., 2021). This accumulation is primarily driven by high N fertilizer inputs, which are motivated by economic incentives to boost orchard yields (Gao, J et al., 2021; Jia et al., 2024; Niu et al., 2022; Yang, Wu, Song, et al., 2020). These findings highlight the need to account for land-use change and its impacts on NO_3^- dynamics, particularly in regions undergoing significant agricultural transformation. While field measurements provide valuable insights into local scale NO_3^- leaching, they are often limited by narrow spatial and temporal coverage. In contrast, numerical modeling and simulations offers a complementary approach to assess long-term NO_3^- transport across larger regions and support evaluations of its potential threat to groundwater quality.

The Guanzhong Plain of China (CGP) is a historically important and intensively farmed agricultural region. Since the 1990s, it has experienced extensive conversion of croplands to orchards, driven primarily by the higher economic returns of orchard crops (Gao, J et al., 2021; Niu et al., 2022; SXBS, 2021). This large-scale land-use transition has raised serious concerns about groundwater NO_3^- contamination, as fertilizer application rates in local orchard systems are far higher than those in traditional croplands (Niu et al., 2022). Notably, as the world's top producer of orchard crops, China applies 1.4 to 9.1 times more fertilizer per unit area in its orchards compared to other major orchard-producing countries (Zhao et al., 2022). Over-fertilization not only increases groundwater pollution risk but also causes substantial economic losses. For this reason, accurately predicting the spatiotemporal dynamics of N in the CGP is critically important. Such reliable predictions can support the development of integrated management strategies, among which reducing excessive fertilization in orchards remains the most direct and effective measure, alongside other practices aimed at balancing energy efficiency and environmental sustainability.

Physically based models of unsaturated flow and solute transport have become vital tools for simulating water and NO_3^- transport processes in the VZ. Among these models, the multi-column approach has been successfully applied in regional-scale soil hydrologic modeling, demonstrating distinct advantages in capturing spatial variability and interactions between hydrological and biogeochemical processes (Hu et al., 2019; Turkeltaub et al., 2018, 2020). This methodology is also integrated into land surface models (e.g., the Community Land Model) to represent soil hydrological dynamics at broader scales (Lawrence et al., 2019). Such physically based models enable the analysis of both individual and combined controls, including soil properties, land-use types, and agricultural management practices, on long-term NO_3^- transport behavior in the VZ. Furthermore, they serve as valuable platforms for exploring various environmental and management scenarios, as well as for evaluating strategies aimed at mitigating groundwater quality degradation (Akbariyeh et al., 2018; Huan et al., 2020; Lyu et al., 2019; Turkeltaub et al., 2018, 2021).

Models simulating water and NO_3^- transport in the VZ rely heavily on accurate soil hydraulic parameters (SHPs), which define the soil water retention and unsaturated hydraulic conductivity functions. Direct measurement of these parameters, however, is often impractical due to high time and resource demands. To address this limitation, researchers commonly use pedotransfer functions (PTFs) to estimate SHPs from easily measurable soil properties (e.g., particle size distribution, bulk density, organic carbon content). This enables the development of regional or

global SHP data sets, providing a practical alternative for model parameterization and supporting large-scale assessments of water and NO_3^- fluxes across agricultural landscapes (Gupta et al., 2021, 2022b; Schaap et al., 2001; Zhang, Y et al., 2018; Zhao et al., 2016). Despite their utility, PTFs have key limitations: many are calibrated for specific geographic and pedoclimatic contexts and may not perform reliably outside their original validation range. Applying such PTFs to regions with dissimilar soil and climate conditions can introduce substantial uncertainties into model predictions (Mohajerani et al., 2021; Paschalis et al., 2022; Weihermüller et al., 2021). It is therefore essential to evaluate how SHP uncertainty affects simulated outputs, using field observations, to improve the reliability of predictions related to groundwater recharge and NO_3^- transport in the VZ.

The primary objective of this study was to apply an established multi-column modeling approach to assess how the conversion of croplands to orchards affects groundwater recharge and NO_3^- transport in the VZ. Simulation uncertainties stemming from SHPs were quantified using an extensive regional database, which includes 124 sampled soil profiles. Based on the modeling results, potential NO_3^- contamination hotspots in the groundwater of the CGP were predicted. This study highlights that, in cultivated loess critical zones (CZs) and other similar regions worldwide, converting croplands to orchards should be accompanied by reduced fertilizer application to minimize the risk of groundwater pollution.

2. Materials and Methods

2.1. Study Area

The study was conducted in the CGP (34°00−35°40 N, 107°30−110°30 E), a 34,000 km^2 region situated in the southern area of the Loess Plateau, within the middle reaches of the Yellow River Basin (Figure 1). The CGP has a sub-humid continental monsoon climate. From 1970 to 2020, the region recorded a mean annual precipitation of 334–900 mm, mean annual temperature of 11.6–14.4°C, and annual potential evapotranspiration of 800–1,100 mm (Figure 2). The groundwater table, an indicator of VZ thickness, varies from 1 to 63 m (median: 24 m) and has remained relatively stable over the past 2 decades (Niu et al., 2022). Known for its fertile soils and favorable climate, the CGP has supported agricultural activity and human settlement for millennia. Historically, its farming systems were dominated by wheat and other cereal crops, with soil fertility maintained primarily through organic amendments (Wang et al., 2017; Wu et al., 2021). Since the 1980s, however, the widespread adoption of chemical fertilizers has fundamentally transformed local agricultural practices (Zhang et al., 1996). Currently, wheat-maize double cropping is the dominant cropping system (Niu et al., 2022). Additionally, since the 1990s, large areas of cropland have been converted to orchards (primarily apple and kiwifruit orchards) to boost economic returns; provincial yearbook data show that orchard coverage in the CGP increased by 48.6% between 1998 and 2020 (SXBS, 2021).

Groundwater is the primary source of agricultural irrigation in the CGP, with furrow irrigation as the dominant method. Under the prevailing winter wheat-summer maize rotation, crops are irrigated five times annually, with a total annual irrigation volume of 300–400 mm (Shen et al., 2020). In contrast, orchards are typically irrigated 3–4 times per year, with total annual irrigation amounts ranging from 400 to 600 mm (Lu et al., 2016). Fertilization rates also differ markedly between the two land-use types: between 2005 and 2009, average annual N inputs reached 440 kg N ha^{-1} yr^{-1} in croplands and 670 kg N ha^{-1} yr^{-1} in orchards (Wang, 2014; Zhao et al., 2014). The CGP's soils are predominantly silty loam and silty clay loam, featuring high porosity and permeability. These favorable hydraulic properties, combined with intensive fertilizer inputs, create conditions that promote significant NO_3^- accumulation in the VZ (Niu et al., 2021, 2022).

2.2. Field Sampling and Laboratory Analysis

In this study, soil and groundwater sampling was conducted to acquire data for model parameterization, calibration, and validation. In 2020, 124 undisturbed soil samples (102 from croplands and 22 from orchards) were collected from the top 0–20 cm soil layer using 100 cm^3 stainless cutting rings. These undisturbed samples were used to measure soil water retention curves (SWRCs), saturated soil hydraulic conductivity (K_s), saturated soil water content (θ_s), and bulk density (BD). Groundwater samples were collected from private wells adjacent to the soil sampling sites, with a total of 124 samples analyzed to determine chloride (Cl^-) concentrations. The locations of all soil and groundwater sites are shown in Figure 1c. Disturbed deep soil samples were collected at 4 field locations (3 in croplands, 1 in orchard) down to a depth of 10 m. These samples were analyzed for particle size

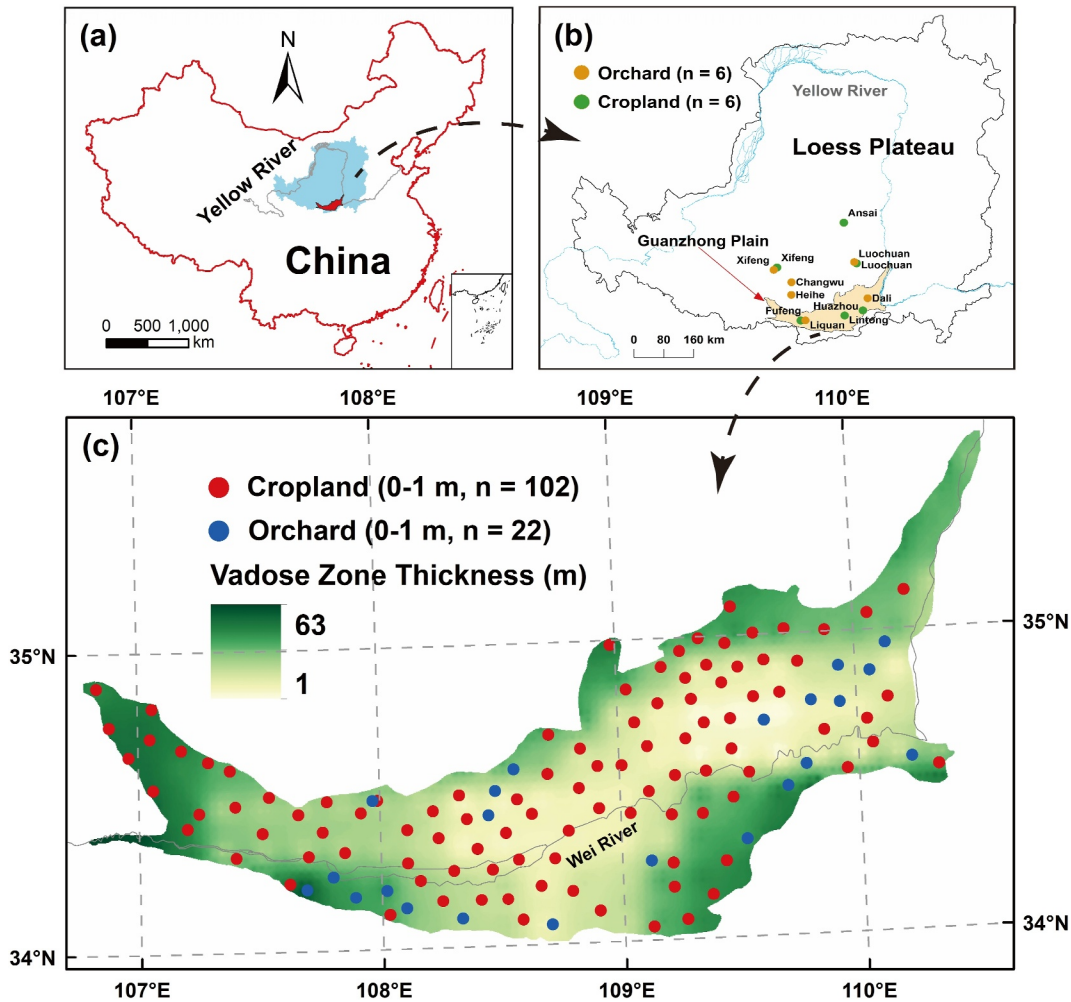

Figure 1. Geographical context and sampling sites. (a) Geographic location of the Guanzhong Plain in China; (b) Spatial distribution of deep soil profiles used for model calibration and validation (Gates et al., 2011; Huang et al., 2018, 2021; Ji et al., 2022; Li et al., 2017; Zhao et al., 2024; Zhu et al., 2023); (c) Spatial distribution of soil and groundwater sampling sites, where red symbols represent croplands and blue symbols represent orchards.

distribution (PSD), Cl^- and NO_3^- content, and soil water content. Sampling intervals were 0–10 cm, 10–20 cm, 20–40 cm, 40–60 cm, 60–80 cm, 80–100 cm, 100–120 cm, 120–160 cm, and 160–200 cm for the upper 2 m, and every 50 cm from 2 to 10 m. To expand the data set for model calibration and validation, 8 additional deep soil profiles from the Loess Plateau were obtained from published literature (Table S1 in Supporting Information S1). Combined with the 4 newly sampled profiles, this yielded a total of 12 soil profiles for model calibration and validation (Figure 1b).

K_s was determined using the constant-head method. In this approach, water flows through a saturated soil column under a steady hydraulic gradient; K_s was then calculated from the measured flow rate (Klute & Dirksen, 1986). SWRC was measured using a high-speed refrigerated thermostatic centrifuge (CR21G, Hitachi, Ltd., Tokyo, Japan) to determine soil water content at varying suction levels (Li et al., 2016). BD was calculated as the ratio of dry soil mass to the core volume. Disturbed soil samples were first air-dried and sieved through a 1 mm mesh. PSD was then analyzed by laser diffraction using a Mastersizer 2000 (Malvern Instruments, Malvern, England). Moist soil samples were extracted with a 2 M potassium chloride (KCl) solution at a soil-to-solution ratio of 1:5. The extracts were filtered through 0.45 μm membranes, and NO_3^- contents were measured using a continuous-flow injection analyzer (FIAstar 5000, FOSS, Denmark). Cl^- content was determined using a discrete chemistry analyzer (Smartchem 200, AMS, Italy). This instrument uses colorimetric analysis, based on the reaction of Cl^- ions with mercury (II) thiocyanate and ferric NO_3^- in an acidic medium. Soil water content was determined

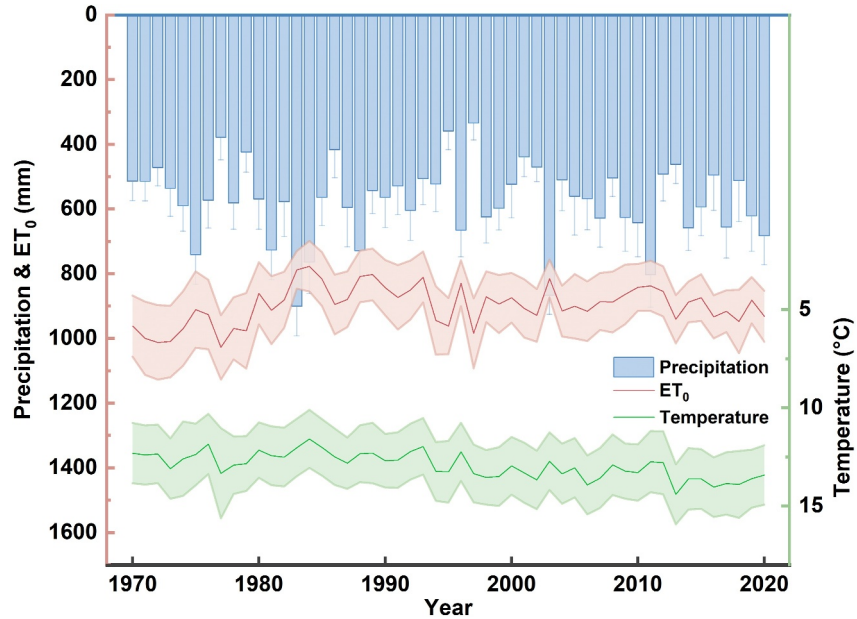

Figure 2. Average annual precipitation, potential evapotranspiration (ET_0), and air temperature in China's Guanzhong Plain (1970–2020). Shaded areas surrounding each trend line represent the range of ± one standard deviation, indicating the interannual variability of each climatic parameter.

gravimetrically: the samples were oven-dried at 105°C for 24 hr, and water content was calculated as the percentage of weight loss relative to the initial wet sample weight.

In addition, farming practices were investigated via field visits, focusing on crop type, irrigation frequency and volume, as well as fertilizer type and application rates. Due to limited data on deep SHPs and the extensive loess coverage, characterized by minimal vertical heterogeneity in the study area (Figure S1 in Supporting Information S1), soil properties in the deep VZ were approximated using data from the 0–20 cm layer. A scaling factor was further used to account for the reduction in hydraulic conductivity with depth (Wang, W et al., 2018). Lateral subsurface flow was not incorporated into the model, as coarse-textured soils are dominant in the study area with flat terrain (Hu et al., 2019). Therefore, it was assumed that water and solute movement is primarily vertical in the VZ of the study area.

2.3. The Multi-Column Modeling Approach

A multi-column modeling approach was employed to simulate regional-scale water and NO_3^- transport in the VZ. This model solves the Richards equation and conservative solute transport equations within a multiple 1D column framework, a method previously validated for applications in loess CZs (Turkeltaub et al., 2018, 2020, 2021). The study area was discretized into multiple 1D vertical columns, with gridded simulations of VZ water and NO_3^- transport driven by spatially gridded variables, including SHPs, land-use type, BD, VZ thickness, daily spatially interpolated meteorological data, irrigation amounts, fertilization rates, leaf area index, single crop coefficients, and Cl^- inputs (Table S2; Figure S2 in Supporting Information S1). Given the relatively uniform soil profiles and flat topography of the region, a representative grid cell spacing of 3,000 m × 3,000 m was adopted, following the approach of Turkeltaub et al. (2018). Details of the specific gridding methodology are provided below.

2.3.1. Soil Hydraulic Parameters, Land Use, and Soil Properties

The SWRC was characterized using the *van Genuchten* equation (van Genuchten, 1980) as follows:

$$\theta(h) = \theta_r + \frac{\theta_s - \theta_r}{(1 + |\alpha h|^n)^{1-\frac{1}{n}}} \quad (1)$$

where $\theta(h)$ is the measured volumetric water content ($L^3\,L^{-3}$) at a pressure head h (L); θ_s is the saturated soil water content ($L^3\,L^{-3}$), which was set to the measured values; θ_r is the residual soil water content ($L^3\,L^{-3}$); α (L^{-1}) is the scaling parameter related to the inverse of the air entry pressure, and n (−) is a curve-shape parameter related to soil pore size distribution.

The unsaturated hydraulic conductivity $K(h)$ is defined as a function of h (van Genuchten, 1980):

$$K(h) = K_s S_e^l \left[1 - \left(1 - S_e^{1/(1-1/n)}\right)^{(1-1/n)}\right]^2 \tag{2}$$

$$S_e = \frac{\theta_s - \theta_r}{\theta - \theta_r} = [1 + (-\alpha h)^n]^{1-\frac{1}{n}} \tag{3}$$

where K_s ($L\,T^{-1}$) is the saturated hydraulic conductivity and l is the soil pore tortuosity parameter with a constant value of 0.5.

The measured θ_s, θ_r, α, n, $K(h)$, and BD were spatially interpolated using the Inverse Distance Weighting (IDW) method to create a 3 km-resolution SHP data set (Data set I). To assess the impact of SHPs uncertainty on simulation accuracy, two additional data sets were used for comparison. Data set II was extracted from a global SHP data set (10 cm depth) developed by Gupta et al. (2020, 2022a) using a random forest-based PTF. SHPs in Data set III were estimated using the RosettaH3 model (Schaap et al., 2001), with input soil properties obtained from the SoilGrid250 m database (10 cm depth; ISRIC, 2017). Both Data sets II and III were resampled to 3 km resolution for consistency. Detailed descriptions of each data set and their spatial distributions are provided in Table S3 and Figures S3 and S4 of Supporting Information S1. All simulations assumed constant SHPs, even though agricultural management practices may cause transient SHP variations. Prior research has shown that such variations are temporary and typically revert to baseline values within a few wetting-drying cycles (Zhang et al., 2017). Given the study's focus on regional-scale hydrological processes, this simplification is deemed reasonable and supports robust qualitative and comparative analyses.

To assess how land-use change affects groundwater recharge and NO_3^- transport in the VZ of the CGP, two hypothetical land-use scenarios (cropland and orchard) were simulated. In the cropland scenario, the entire study area was assumed to be cropland under a wheat-corn rotation: wheat (October–May) and corn (June–September). Irrigation and fertilization were applied three times for wheat (December, March, May) and twice for corn (June, July). In the orchard scenario, the entire study area was assumed to be orchards, represented by apple trees (a dominant local orchard crop; Table S4 in Supporting Information S1). As perennial systems, apple orchards were simulated as year-round vegetation. Irrigation and fertilization were scheduled four times annually (April, June, July, August), consistent with regional orchard management norms. Land-use data were derived from the *China Multi-Period Land Use Remote Sensing Monitoring Data set* (Xu et al., 2018). VZ thickness data were sourced from the *Global Groundwater Table Distribution Data set* (Fan et al., 2013), which is built on over 1 million well records. Its accuracy in the CGP was validated against published groundwater depth contour maps (Zhang, 2018), showing good agreement in both spatial distribution and depth range (VZ thickness across the region: 1.0–63 m).

2.3.2. Climate Data

Daily meteorological variables were collected from 31 meteorological stations in the CGP over the period 1970–2020 (Figure 2, Figures S5 and S6 in Supporting Information S1). The variables include daily mean, maximum, and minimum air temperature (°C), daily precipitation (mm), relative humidity (%), sunshine hours (h), and wind speed ($m\,s^{-1}$). For each meteorological station, daily reference evapotranspiration (ET_0) was calculated using the Penman-Monteith equation (Allen et al., 1998). To match the model's 3 km grid resolution, spatial interpolation of key daily climatic variables (precipitation, mean air temperature, and ET_0) from the 31 stations was performed using the IDW method.

2.3.3. Leaf Area Index (LAI) and Chloride Data

LAI (a key parameter for simulating vegetation water use) and single crop coefficients (used to calculate actual ET) were assigned based on measured values from published literature (Kang et al., 2003; Liu et al., 2012). These parameters were further gridded according to land-use type (cropland vs. orchard) and set to vary with time,

reflecting seasonal changes in crop growth. Cl^- was used as a conservative tracer to constrain water flow simulations, with inputs derived from three sources: precipitation, irrigation, and dry deposition. The Cl^- concentration in precipitation (including contributions from dry deposition) was estimated using a linear regression equation:

$$Cl_c = -0.001 \times P + 1.618 \tag{4}$$

where Cl_c is the Cl^- concentration in precipitation (mg L^{-1}) and P is precipitation amount (mm). This equation was developed from long-term monitoring of precipitation Cl^- concentrations in the study region and has been validated to effectively capture Cl^- inputs from both wet precipitation and dry deposition (Li et al., 2017), ensuring high reliability for regional-scale simulations.

Groundwater is the primary source of irrigation water in the CGP (SPWRD, 2018; Wang, H et al., 2018). Thus, the Cl^- concentration in irrigation water was determined using gridded groundwater Cl^- data. This gridded data set was generated by spatially interpolating Cl^- concentration measurements from 124 groundwater sampling sites via the IDW method, matching the model's 3 km grid resolution.

2.4. Model Setup

2.4.1. Water Flow and Solute Transport Models

Unsaturated water flow and NO_3^- transport in the VZ were simulated using the Hydrus-1D code (Šimůnek et al., 2008). For the unsaturated flow module, the simulation was governed by the Richards equation:

$$\frac{\partial \theta}{\partial t} = \frac{\partial}{\partial z}\left[K\left(\frac{\partial h}{\partial z} + 1\right)\right] - S \tag{5}$$

where h (L) is the pressure head, θ ($L^3\ L^{-3}$) is the volumetric water content, t (T) is time, z (L) is the vertical coordinate, K ($L\ T^{-1}$) is the unsaturated hydraulic conductivity function, and S is a root water uptake sink term (T^{-1}).

N transport in the soil is primarily driven by two processes: advection and dispersion. To account for N transformations (e.g., mineralization, immobilization, denitrification) during transport, a first-order reaction kinetic equation was adopted, following the approach of Turkeltaub et al. (2018). This equation is expressed as:

$$\frac{\partial \theta C_{NH_4}}{\partial t} + \frac{\partial \rho S_{NH_4}}{\partial t} = \frac{\partial}{\partial z}\left[\theta D \frac{\partial \theta C_{NH_4}}{\partial z}\right] - \frac{\partial q C_{NH_4}}{\partial z} - f_{NH_4} S C_{NH_4} - \mu_{nit} \theta C_{NH_4} - \mu_{vol} \theta C_{NH_4} \tag{6}$$

$$S_{NH_4} = K_d C_{NH_4} \tag{7}$$

$$\frac{\partial \theta C_{NO_3}}{\partial t} = \frac{\partial}{\partial z}\left[\theta D \frac{\partial \theta C_{NO_3}}{\partial z}\right] - \frac{\partial q C_{NO_3}}{\partial z} - f_{NO_3} S C_{NO_3} + \mu_{nit} \theta C_{NH_4} \tag{8}$$

where C_{NH4} and C_{NO3} (M L^{-3}) are concentrations of the N species in the pore-water solution; S_{NH4} (M M^{-1}) is the mass fraction of the adsorbed NH_4; ρ (M L^{-3}) is the soil's bulk density; θ ($L^3\ L^{-3}$) is volumetric water content; D ($L^2\ T^{-1}$) is the hydrodynamic dispersion coefficient; q ($L\ T^{-1}$) is the water flux; $f_{NH4}SC_{NH4}$ and $f_{NO3}SC_{NO3}$ (M $T^{-1}\ L^{-3}$) are the root NH_4 and NO_3 uptake sinks, respectively, where f_{NH4} and f_{NO3} are functions relating solute uptake to the water uptake S and solute concentrations; μ_{nit} (T^{-1}) is a first-order nitrification rate; μ_{vol} (T^{-1}) is NH_4 volatilization rate; and K_d ($L^3\ M^{-1}$) is the NH_4 partition coefficient. The values of μ_{vol}, μ_{nit}, and S_{NH4} refer to previous research (Akbariyeh et al., 2018).

The hydrodynamic dispersion coefficient depends on both water velocity and water content, and is calculated as follows:

$$D = \lambda v + D_w \tau_w \tag{9}$$

where D_w is the molecular diffusion coefficient in free water ($L^2\ T^{-1}$); τ_w is a tortuosity factor in the liquid phase (−); v is the pore water velocity ($L\ T^{-1}$); and λ is the longitudinal dispersity (L). The tortuosity factor ($\tau_w = \frac{\theta^{7/3}}{\theta_s^2}$) was delineated by Millington and Quirk (1961), and the value of D_w ($1.52 \times 10^{-4}\ m^2\ day^{-1}$) was obtained from previous literature (Lide, 2002).

2.4.2. Root Distribution Models

The root water uptake rate (sink term) was simulated using the *Feddes* equation (Feddes et al., 1978):

$$S(h) = F(h)\, S_p \tag{10}$$

where $F(h)$ is the dimensionless coefficient of root water uptake ($0 \le F \le 1$) and S_p is the potential water uptake (T^{-1}). The root water uptake parameter of the *Feddes* equation for orchards and croplands was adopted from Baram et al. (2016) and Ma et al. (2011). Root water uptake occurred simultaneously with root N uptake. We assumed passive N uptake by roots and set the maximum allowable concentration for root N uptake (Table S5 in Supporting Information S1).

In a 1D system, the potential root water uptake, S_p is described by Feddes et al. (1978):

$$S_p(z) = \frac{\beta(\mathrm{z})\, T_p}{\int_0^{Z_m} \mathrm{F(h)}\, dz} \tag{11}$$

where β(z) is a function (L^{-1}) describing the root distribution with depth; T_p is the potential transpiration rate ($L\ T^{-1}$); and Z_m is the maximum rooting depth (L). The 1D root depth distribution model was proposed by Vrugt et al. (2001) and based on the model by Raats (1974):

$$\beta(\mathrm{z}) = \left[1 - \left(\frac{z}{z_m}\right)\right] e^{-\frac{P_z}{z_m}|z^* - z|} \tag{12}$$

where z represents depth (L); Z_m represents maximum rooting depth (L); and P_z and z*(L) are empirical parameters.

In the CGP, wheat and maize roots are predominantly distributed within the 0–1 m soil depth (Wang, Y et al., 2015), whereas 90% of apple roots are concentrated in the 0–2 m soil layer (Li et al., 2019). Consequently, root depth was set to 0–1 m for croplands and 0–2 m for orchards. Regarding solute transport parameters, initial values for P_z (a parameter related to preferential flow or solute partitioning) and z* (a depth-related scaling parameter for solute processes) were first determined based on values reported in previous studies (Vrugt et al., 2001). These initial values were further calibrated and adjusted using measured soil NO_3^- content data, following the parameter optimization approach of Turkeltaub et al. (2018).

2.4.3. Initial and Boundary Conditions

To establish realistic simulation start stages, the model was initialized with two key settings: soil moisture set to field capacity and all solute (NO_3^-, ammonium, and Cl^-) concentrations set to zero. The initial run's outputs served as the baseline for three subsequent 18,628-day iterations. The first two iterations acted as spin-up to equilibrate the system and reach dynamic steady state. Only results from the final iteration were used for analysis, ensuring outputs reflect long-term stable system behavior rather than transient initial conditions.

The upper boundary is an atmospheric boundary condition incorporating surface runoff, which accounts for water inputs (precipitation, irrigation) and outputs (ET, runoff) at the soil surface. The lower boundary, located at the groundwater table (submerged surface), is set as a constant head boundary. For solute transport, the upper boundary is a concentration flux boundary that specifies solute inputs (e.g., NO_3^- from fertilization, Cl^- from precipitation/irrigation) entering the soil surface. The lower boundary is a zero-concentration gradient boundary, which means no net solute flux occurs across the VZ base. The length of each simulated 1D soil column was matched to the thickness of the VZ at each grid cell.

The model received daily time-step inputs to drive water and solute dynamics, including water inputs (precipitation and irrigation), crop-related parameters (LAI, pET_0), and solute inputs (concentrations of Cl^- and ammonium). The amounts and frequencies of irrigation were derived from previous literature (Huang et al., 2004; Kang et al., 2017). Croplands were further categorized into irrigated and non-irrigated (rain-fed) systems to reflect real management variability. pET_0 was calculated by multiplying ET_0 (reference evapotranspiration) by a single crop coefficient.

In recent decades, N fertilizer application in the CGP has increased at an annual rate of 4.14%, though this trend is not statistically significant (Gao, Y et al., 2021). Due to the lack of precise data on this topic, the average annual N fertilizer application to orchards and croplands in each county was calculated using literature and on-site investigation results (Gao, Y et al., 2021; Figure S7 in Supporting Information S1). In this study, both synthetic and organic fertilizers (e.g., livestock manure, human waste) were included as N inputs in the model, with ammonium bicarbonate being the predominant synthetic fertilizer in the region. Previous studies have shown that N inputs from anthropogenic sources did not exceed plant uptake before the 1980s (Bouwman & Boumans, 2002; Zhang et al., 1996); thus, fertilizer application data were only incorporated into regional-scale models after this period.

To assess the effects of land use on groundwater recharge and NO_3^- transport patterns in the CGP, two hypothetical land-use scenarios (cropland and orchard) were simulated. Each scenario was run with three distinct SHP data sets, resulting in a total of six simulations (C1, C2, C3, O1, O2, O3), where "C" denotes cropland and "O" represents orchard.

2.5. Model Calibration and Validation

Cl^- is highly hydrophilic and chemically stable, making it a reliable tracer for soil water fluxes (Niu et al., 2022). To accurately capture water flow and NO_3^- transport in the deep VZ, the regional-scale model was calibrated and validated using measured Cl^- and NO_3^- contents. Model calibration involved adjusting parameters related to longitudinal dispersion, root water uptake, and root distribution, based on two soil profiles collected from distinct locations in the study area (Lintong and Luochuan). Validation was then conducted using measured Cl^- and NO_3^- contents from 12 profiles: 4 collected in the CGP and 8 from loess regions surrounding the CGP (Gates et al., 2011; Huang et al., 2018, 2021; Ji et al., 2022; Li et al., 2017; Zhao et al., 2024; Zhu et al., 2023; see Figure 1b). Specifically, 10 NO_3^- profiles were sampled from 5 apple orchards and 5 wheat-corn rotation croplands, while 6 Cl^- profiles were sampled from 3 apple orchards and 3 wheat-corn rotation croplands (Figure 1b). For each profile simulation, measured soil parameters were used, and initial and boundary conditions were set as described in Section 2.4.3. To account for uncertainty in Cl^- and NO_3^- inputs, the model was run 15 times; for each run, fertilizer application amounts, irrigation amounts, and Cl^- inputs were randomly generated within a ±20% range of their reference values. Simulation results are presented as concentration ranges for NO_3^- and Cl^- profiles.

2.6. Statistical Analysis

2.6.1. Sensitivity Analysis

The model sensitivity to SHPs was quantified using the following sensitivity coefficient (Xia, 2008):

$$A = \frac{\Delta Y/Y}{\Delta X/X} \times 100\% \tag{13}$$

where A is the sensitivity coefficient; Y is the objective variable; ΔY is the quantity of change in the objective variable; X is the independent variable; ΔX is the quantity of change in the independent variable. A positive value of A indicates that Y and X changed in the same direction.

To assess how SHPs influence the model's performance, sensitivity analyses were performed using the one-factor-at-a-time approach (Hu et al., 2019). With all other parameters held constant, each SHP was adjusted individually within a ±10% range of its base simulated value. Model sensitivity coefficients for each SHP were then calculated based on the results of these adjustments.

2.6.2. Uncertainty Analysis

To assess potential uncertainties caused by differences in SHP data sets, a quantitative uncertainty coefficient (σ) was calculated following the method by Paschalis et al. (2022):

$$\sigma = \frac{\sqrt{\left(\frac{1}{n-1}\sum_{i=1}^{n}\left[Y-\overline{Y}\right]^2\right)}}{\overline{Y}} \tag{14}$$

where n denotes the number of SHPs data sets; Y denotes the simulation results of the regional-scale model; and $\overline{Y}$ denotes the average value of all regional-scale simulation results.

Due to the limited availability of high-quality fertilization and irrigation records, regional-scale uncertainties in these inputs could not be explicitly constrained. Instead, uncertainty propagation was evaluated using 12 observational profiles: fertilization and irrigation rates were perturbed within a ±20% range of their reference values, and 15 independent model realizations were conducted with randomly generated parameter combinations to systematically assess the variability of results induced by these perturbations.

2.6.3. Model Accuracy Evaluation

The accuracy of the model was evaluated using four metrics: Nash-Sutcliffe Efficiency (NSE), Pearson correlation coefficient (r), root-mean-square error (RMSE), and *bias*. Their respective calculation formulas are as follows:

$$\mathrm{NSE} = 1 - \frac{\sum_{i=1}^{n}\left(o_i - p_i\right)^2}{\sum_{i=1}^{n}\left(o_i - \overline{o}\right)^2} \tag{15}$$

$$r = \frac{\sum_{i=1}^{n}\left(p_i - \overline{p}\right)\left(o_i - \overline{o}\right)}{\sqrt{\sum_{i=1}^{n}\left(p_i - \overline{p}\right)^2}\sqrt{\sum_{i=1}^{n}\left(o_i - \overline{o}\right)^2}} \tag{16}$$

$$\mathrm{RMSE} = \sqrt{\frac{1}{n}\sum_{i=1}^{n}\left(p_i - o_i\right)^2} \tag{17}$$

$$\mathrm{bias} = \frac{1}{n}\sum_{i=1}^{n}\left(p_i - o_i\right) \tag{18}$$

where p_i and o_i represent the predicted and measured values, respectively; n represents the number of samples; $\overline{p}$ is the average value of all predicted values (p_i); and $\overline{o}$ is the average value of all measured values (o_i).

3. Results and Discussion

3.1. Model Performance

Figure 3 presents representative Cl^- and NO_3^- profiles sampled from different sites and their corresponding simulated values. For most locations, high Cl^- content was measured within the 0–6 m depth, with a substantial decline in Cl^- content in deeper soil layers (Figure 3). This phenomenon of high Cl^- accumulation in the upper unsaturated zone has been previously reported in the region (Huang et al., 2018, 2021) and is mainly attributed to evapotranspiration-driven accumulation processes during continuous deposition events (Gates et al., 2011). Since infiltration from precipitation and irrigation primarily affects upper soil layers, Cl^- is not efficiently leached to deeper layers (Li et al., 2017). In orchards, significant Cl^- accumulation in shallow soils may be indicative of intensive evapotranspiration (due to the high water demand of orchard trees), high Cl^- content in irrigation water, or a combination of both factors (Min et al., 2018; Turkeltaub et al., 2014). Moreover, the observed Cl^- profiles in orchards, characterized by sharper peaks, are best explained by preferential flow processes. The dense, deep root systems of orchards promote the development of preferential paths, allowing solutes to rapidly bypass the upper soil matrix (Beven & Germann, 2013; Jarvis, 2020; Zhang et al., 2019). This contrast in flow regimes becomes

10.1029/2025WR040349

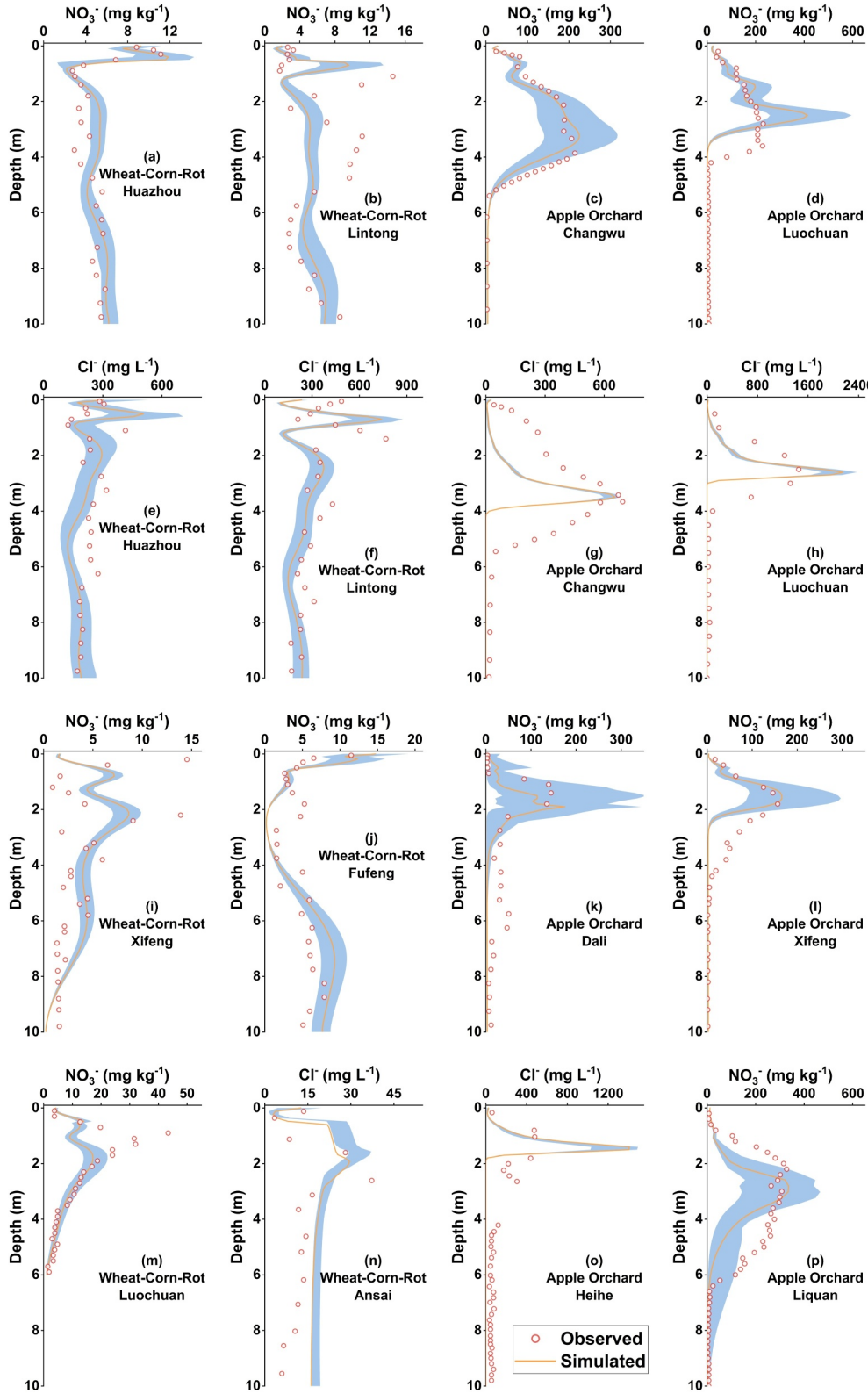

Figure 3. Measured and simulated Cl^- and NO_3^- content along soil profiles. The shaded areas represent the ranges derived from 15 simulations, which account for random variations in fertilizer and irrigation amounts as well as Cl^- input.

more pronounced below the root zone, where piston flow dominates downward movement slows significantly, concentrating Cl^- into a steep gradient at the root zone's base. Below 6 m, Cl^- contents in orchard profiles decreased sharply and stabilized at approximately 23.8 mg L^{-1}, as seen in data from sites such as Changwu and Luochuan (Figures 3g and 3h). By comparison, agricultural fields at the same sites had even lower Cl^- content in soil layers deeper than 6 m, with an average of 10.3 mg L^{-1} (Huang et al., 2018, 2021), suggesting that Cl^- accumulation persisted after the conversion of croplands to orchards (Huang & Pang, 2011). Higher Cl^- content was observed in the 0–1 m layer of cropland profiles at the Huazhou and Lintong sites (Figures 3e and 3f), but this is likely due to soil profile measurements being conducted immediately after irrigation events (Turkeltaub et al., 2018).

Analysis of 10 representative NO_3^- profiles revealed a significant difference in the upper 10 m of soil between croplands and orchards (Figure 3). The mean NO_3^- content in cropland soil (6.3 mg kg^{-1}) is significantly lower than that in orchard soil (67.5 mg kg^{-1}) (Figure 3). These findings are consistent with previous studies on the Loess Plateau (Fan et al., 2024; Li et al., 2011; Niu et al., 2022; Tian et al., 2024), which provide strong evidence for land-use transition's impact on soil NO_3^- levels. Notably, NO_3^- content in orchard profiles consistently peaked at shallow depths (0–4 m), a pattern similar to that of Cl^- profiles, implying the potential involvement of shared regulatory mechanisms. In cultivated soils, NO_3^- primarily originates from fertilizer inputs (Ascott et al., 2017). In shallow soil layers, NO_3^- gradually accumulates under the combined effects of irrigation, precipitation, and evapotranspiration, processes that also facilitate its movement to deeper layers. However, constrained by lower drainage rates in deeper soil and limited infiltration depth of precipitation, NO_3^- movement slows below 4–6 m. It then migrates downward gradually via the piston flow of soil water, ultimately reaching groundwater (Huang et al., 2013, 2018). At the Huazhou, Fufeng, and Xifeng sites, higher NO_3^- content was observed in the 0–1 m topsoil than in deeper layers of cropland profiles (Figures 3a, 3i and 3j). This pattern is likely explained by soil profile measurements being conducted immediately after fertilization events (Turkeltaub et al., 2018), before the newly applied NO_3^- had time to leach to lower soil layers.

A comparison of simulated and measured Cl^- and NO_3^- content showed broad structural agreement across most profiles (Figure 3). This was further supported by scatter plots of simulated versus observed values, which revealed reasonable correlations for both Cl^- ($r = 0.65$) and NO_3^- ($r = 0.81$) (Figure S8 in Supporting Information S1). Nevertheless, localized deviations persisted at certain depths in several profiles. Overall, both solutes exhibited similar simulation performance within the same profile (Figures 3a–3h). For instance, the model successfully reproduced the depth distributions of Cl^- and NO_3^- at the Huazhou site (Figures 3a and 3e). By contrast, it overestimated the peak concentrations of both solutes at the Luochuan orchard site (Figures 3d and 3h), a discrepancy likely tied to the site's historical transition from cropland to orchard. Since the model did not account for temporal dynamics in land-use practices and instead simulated the site as an orchard throughout the study period, it failed to reflect the lower residual solute levels associated with prior cropland use, leading to overestimated cumulative peaks. A similar explanation applies to the Heihe site (Figure 3o). Conversely, at the Luochuan cropland site (Figure 3m), NO_3^- peaks were underestimated. This may stem from the simulation only considering continuous cropland use, omitting intermediate land-use transitions that could have contributed to NO_3^- accumulation. At the Changwu site (Figures 3c and 3g), while NO_3^- profiles were well captured, the Cl^- peak width was underestimated, a discrepancy potentially linked to the model's simplified representation of preferential flow. As a conservative tracer, Cl^- transport is primarily controlled by water flow and thus more sensitive to simplified hydraulic representations, often resulting in sharper simulated peaks. In contrast, the distribution of reactive N is also influenced by root uptake and nitrification processes, which may offset structural inaccuracies in transport parameterization. At other sites, including Lintong (Figure 3b), Xifeng (Figures 3i and 3l), Liquan (Figure 3p), and Ansai (Figure 3n), discrepancies may arise from the model's assumption of vertically homogeneous soil properties (e.g., hydraulic parameters and bulk density), which neglects natural soil layering and heterogeneity (Turkeltaub et al., 2018). Additionally, the elevated topsoil NO_3^- content observed at the Xifeng cropland site (Figure 3i) may be attributed to recent fertilization. This transient peak could not be accurately captured in the simulation, as site-specific fertilization records were unavailable and data were sourced from previous literature.

Discrepancies between simulated and observed values at specific depths and sites may also stem from uncertainties in input parameters, which govern key processes such as solute transport, water redistribution, and root water uptake. For instance, an underestimated longitudinal dispersity could dampen simulated water and solute movement to deeper layers, while inaccurate root distribution parameters might distort the spatial pattern of water

uptake in the VZ. Optimal model parameters were determined as follows: longitudinal dispersity (λ) was 0.075 m. For the wheat-corn rotation system, the root distribution parameters Z^* and P_z were 0.45 m and 4.53, respectively; for orchard systems, these parameters were −0.1 m and 0, respectively.

We acknowledge that certain inherent model assumptions, alongside uncertainties in input data and parameters, may influence simulation results. This study focused on assessing the impacts of regional-scale agricultural land-use change from croplands to orchards on groundwater recharge and NO_3^- transport. At this regional scale, obtaining all model parameters via experimental measurements is impractical, particularly for biogeochemical reactive parameters. We made efforts to acquire and estimate representative parameters for simulating both cropland and orchard systems in the study area, and these limitations do not undermine the significance of the study's conclusions. We consider the assumptions and data used in the current model to be appropriate for the research context. Importantly, the alignment between simulated results and observed data supports the accuracy of the model setup, reinforcing confidence in the insights derived from this work.

3.2. Impacts of SHPs on Model Prediction

To assess how SHP variability influences regional-scale simulations of VZ water flow and NO_3^- transport, the model was run using two additional widely adopted SHP data sets. The reliability of Data set I (measured SHPs) was verified by comparing it with SHPs reported in other studies (Bai et al., 2022; Qiao et al., 2018; Zhao et al., 2016). Notable variations were observed across all three SHP data sets: Data set I exhibited greater spatial heterogeneity than Data sets II and III (both model-estimated SHPs), as illustrated in Figures S3 and S4 of Supporting Information S1.

The results showed similarities in the spatial distribution of groundwater recharge flux, NO_3^- leaching flux and rate, and NO_3^- travel time across the three SHP data sets. However, under the orchard scenario, Data sets II and III failed to capture hotspots of high groundwater recharge flux, high NO_3^- leaching flux and rate, and distinct NO_3^- travel times (Figures S9–S12 in Supporting Information S1). This discrepancy is likely attributed to the reduced spatial heterogeneity in Data sets II and III: their standard deviations were 50%–98% lower than those of Data set I (Table S6 in Supporting Information S1). This lack of variability limited their ability to accurately represent localized differences in water flow and NO_3^- transport processes, key to identifying hotspots in the orchard scenario (Figure S3 in Supporting Information S1).

The uncertainty analysis results highlight the critical impact of SHPs on simulations of water flow and NO_3^- transport in the VZ, with a particular influence on NO_3^- leaching fluxes. In the orchard scenario, SHPs induced an uncertainty of 44.9% in NO_3^- leaching fluxes; in the cropland scenario, this SHP-driven uncertainty was even higher, reaching 86.3% (Figure 4). Additionally, variations in SHPs led to a significant 44.8% variation in the simulated groundwater recharge fluxes under the orchard scenario.

Overall, the effect of SHPs on water flow and NO_3^- transport is significantly stronger in orchards than in croplands, which is also supported by the sensitivity analysis (Table 1) The primary driver of this difference lies in how SHP uncertainty propagates through root-zone water distribution, a process that directly regulates root water uptake. Orchards, which typically have deeper and denser root systems, are disproportionately sensitive to variations in root-zone water availability caused by SHP differences. This heightened sensitivity translates to greater variability in both water and solute fluxes in orchard simulations. While fully characterizing soil heterogeneity remains impractical, refining the precision and spatial coverage of SHP data is a critical step toward reducing systematic model bias and improving the representation of local-scale hydrological and biogeochemical dynamics. Consequently, constructing robust SHP data sets in data-sparse regions is vital for enhancing the reliability of VZ and groundwater models.

3.3. Groundwater Recharge Under Two Land Use Scenarios

As depicted by simulations using measured SHPs, the average annual groundwater recharge flux in the CGP exhibits a distinct spatial pattern, with higher recharge in the eastern region and lower in the western region (Figures 5a and 5b). This east–west gradient in groundwater recharge can be attributed to two key hydrogeological and soil properties in the CGP: the eastern region is dominated by sandy soil (which facilitates more rapid infiltration) and features a shallower groundwater table (reducing the vertical distance water must travel to reach the aquifer) (Figure 1c and Figure S13 in Supporting Information S1; Cao et al., 2016; Fu et al., 2019).

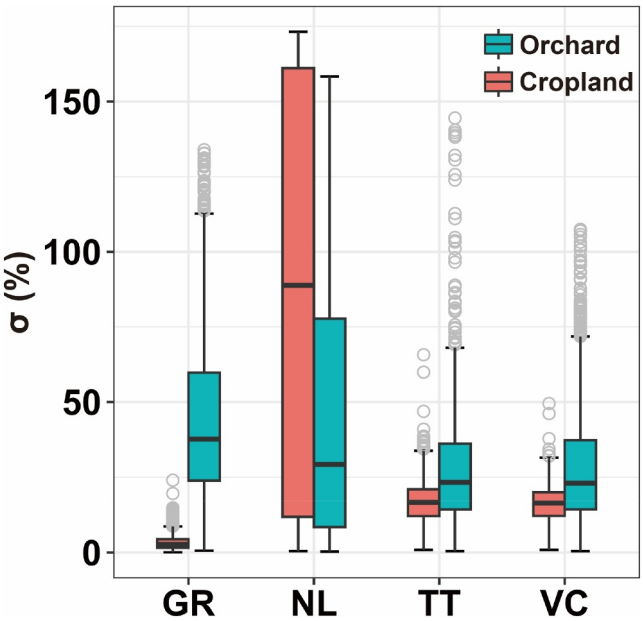

Figure 4. Boxplots illustrating uncertainties in water and NO_3^- transport simulations introduced by pedotransfer functions for cropland and orchard. GR: groundwater recharge flux (mm yr^{-1}), NL: NO_3^- leaching flux (kg ha^{-1} yr^{-1}), TT: NO_3^- travel time (yr), VC: velocity (mm yr^{-1}).

Simulations indicated that converting croplands to orchards reduced the average groundwater recharge rate in the CGP by 10%, from 167 ± 27 mm yr^{-1} in croplands to 151 ± 95 mm yr^{-1} in orchards. This finding aligns with previous studies (Huang et al., 2018, 2021), which attribute the recharge decline to orchards' higher water uptake and deeper root distribution, both of which increase overall water consumption (Jia et al., 2017; Li et al., 2018; Zhang, Z et al., 2018). The larger standard deviation in orchard recharge rates reflects greater spatial variability, a pattern linked to the model's heightened sensitivity to SHPs when simulating orchard systems (Table 1). Specifically, the model was most sensitive to changes in two *van Genuchten* equation parameters: θ_s ($A = -1.25$) and n ($A = 1.12$). Spatial heterogeneity in orchard groundwater recharge was primarily driven by variation in θ_s (Figure S3 in Supporting Information S1). Overall, the cropland-to-orchard shift not only reduces groundwater recharge but also increases irrigation demand. The resulting greater reliance on groundwater pumping exacerbates aquifer depletion, raising critical concerns for long-term groundwater sustainability in the CGP.

3.4. NO_3^- Transport Under Two Land Use Scenarios

Under the cropland scenario, simulation results indicated that NO_3^- leaching fluxes averaged approximately 5 ± 7 kg ha^{-1} yr^{-1}. Hotspots of elevated NO_3^- leaching were predicted in the central and eastern regions of the CGP (Figure 6a), a pattern likely driven by higher fertilizer application rates and presence of coarse sediments (Figures S7 and S13 in Supporting Information S1; Green et al., 2008).

Simulations indicated that converting croplands to orchards in the CGP significantly amplified NO_3^- leaching, with fluxes increasing 38-fold, from the cropland baseline to 192 ± 109 kg ha^{-1} yr^{-1} (Figures 6a and 6b). This substantial increase reflects the combined influence of three key factors: intensive irrigation practices, high fertilizer application rates, and distinct root distribution patterns in orchards (Gao, J et al., 2021; Maharjan et al., 2014; Niu et al., 2022). While NO_3^- leaching fluxes in both cropland and orchard systems were sensitive to SHPs, particularly θ_s (average sensitivity coefficient of 1.48) and n (1.89), orchards exhibited stronger spatial heterogeneity in leaching. This suggests that fertilizer management, when combined with SHP variability, acted as a key control on orchard NO_3^- leaching (Figure S7 in Supporting Information S1). Moreover, groundwater

Table 1
Sensitivity Analysis of Soil Hydraulic Parameters (SHPs) for Key Indicators Under Crop and Orchard Scenarios

Indicators	Scenarios	θ_r	θ_s	α	n	K_s
Groundwater recharge (mm yr^{-1})	Crop	0.03	−0.27	0.06	0.44	0.03
	Orchard	0.17	**−1.25**	0.23	**1.12**	0.06
NO_3^- leaching (kg ha^{-1} yr^{-1})	Crop	−0.07	**−3.20**	0.17	**4.27**	0.35
	Orchard	0.09	−0.78	0.12	0.82	0.04
Velocity (mm yr^{-1})	Crop	−0.06	**−1.17**	0.06	**1.69**	0.14
	Orchard	0.03	**−2.03**	0.21	**2.50**	0.16
Travel time (yr)	Crop	0.06	**1.15**	−0.06	**−1.71**	−0.14
	Orchard	−0.03	**1.98**	−0.22	**−2.56**	−0.16

Note. θ_r: cm^3 cm^{-3}; θ_s: cm^3 cm^{-3}; α: cm^{-1}; n: –; K_s: saturated hydraulic conductivity (cm min^{-1}). The values presented in the table represent the sensitivity coefficient (A), which quantifies the percentage change in the simulated indicator induced by a 1% change in the corresponding SHP. When $A > 0$, it signifies a positive correlation between the SHP and the indicator; conversely, when $A < 0$, it signifies a negative correlation. The greater the absolute value of A, the higher the sensitivity of the model to the corresponding SHP. Values for which the absolute value of A exceeds 1 are presented in bold to emphasize parameters to which the model displays heightened sensitivity, thereby facilitating the visual identification of key sensitivities.

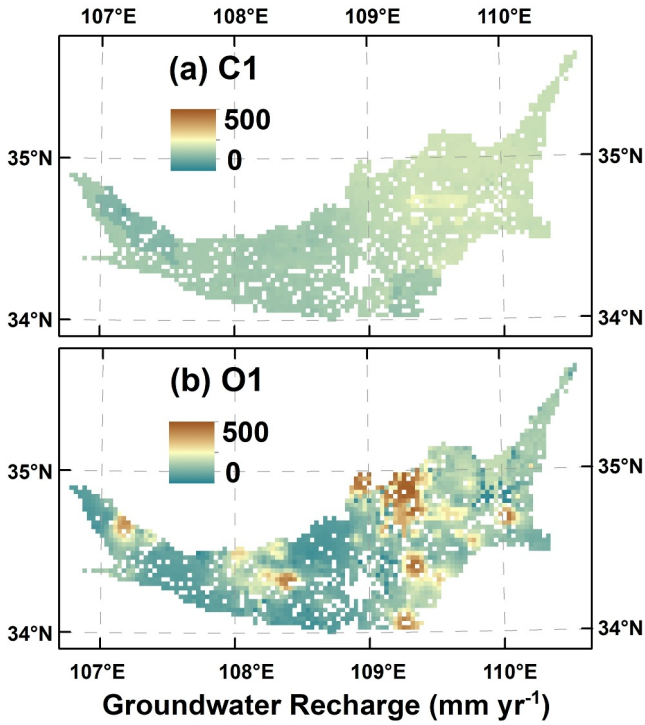

Figure 5. Distribution of groundwater recharge fluxes under two land-use scenarios, which are based on simulations of measured SHPs (Data set I). C1: Cropland scenario; O1: Orchard scenario.

recharge further modulated the spatial pattern of NO_3^- leaching fluxes, as water flow through the VZ directly governs the transport of dissolved NO_3^- (Ascott et al., 2017). Collectively, these findings demonstrate that the spatial distribution of NO_3^- leaching fluxes is shaped by the interplay of multiple factors: SHPs, fertilizer management, and groundwater recharge dynamics. Notably, previous studies have reported contrasting results regarding cropland-to-orchard impacts on NO_3^-. For instance, Lu et al. (2015) observed a decline in soil N following this land-use transition. This discrepancy arises because the orchards in their study were unfertilized, whereas the CGP orchards in our simulation rely on intensive fertilization. This contrast highlights the central role of fertilization practices in driving NO_3^- leaching, reinforcing that high nutrient inputs are a prerequisite for the substantial leaching increases observed in the CGP orchard scenario.

NO_3^- leaching rate and travel time through the VZ are key indicators of groundwater NO_3^- pollution risk. NO_3^- leaching rates in this study were estimated based on groundwater recharge rates and soil profile water content (Turkeltaub et al., 2018). Consistent with the spatial pattern of groundwater recharge, NO_3^- leaching rates exhibited an east–west gradient: rates were higher in the eastern CGP and lower in the western region. The transition from croplands to orchards reduced the average NO_3^- leaching rate by 11% (from 459 ± 83 mm yr^{-1} in croplands to 408 ± 210 mm yr^{-1} in orchards), with orchards showing larger spatial heterogeneity in leaching rates (Figures 6c and 6d). The mechanisms driving this greater variability in orchard NO_3^- leaching rates mirror those identified for groundwater recharge: heightened sensitivity to SHP variability and the influence of orchard-specific root water uptake patterns.

NO_3^- travel time in the VZ, calculated using VZ thickness and NO_3^- leaching rates, ranged from several decades to hundreds of years across the study area (Figures 6e and 6f). The spatial pattern of travel time was similar under cropland and orchard scenarios, with two hotspots of faster NO_3^- transport in the central and eastern CGP. These hotspots coincided with areas of high NO_3^- leaching and generally matched locations of elevated groundwater NO_3^- concentrations in the CGP reported by Niu et al. (2022), a consistency that supports the model's validity. The shortest NO_3^- travel times occurred in regions with a thinner VZ, as the shorter vertical distance reduced the time required for NO_3^- to reach the aquifer. The transition from croplands to orchards extended average NO_3^- travel time by 23 years, increasing it from 58 ± 36 years (croplands) to 81 ± 68 years (orchards). Previous studies have emphasized that groundwater quality changes lag behind land-use changes (Huang et al., 2013), and this cropland-to-orchard shift exacerbates this delay. Importantly, however, denitrification (a process that reduces NO_3^- to inert gases) is weak in the semi-arid CGP (Niu et al., 2022; Wang et al., 2019), meaning most NO_3^- entering the VZ will eventually reach groundwater. Model simulations further revealed an 18-fold increase in NO_3^- storage in the VZ under orchards: from 2,647 kg N ha^{-1} in croplands to 47,542 kg N ha^{-1} in orchards (Figure S14 in Supporting Information S1). For croplands, the simulated mean NO_3^- storage in the 0–10 m soil layer (1,198 kg N ha^{-1}) closely matched field observations (1,243 kg N ha^{-1}; Niu et al., 2022), providing additional validation of the model. Although the large NO_3^- stores in the VZ will not enter groundwater immediately due to long travel times, they represent a long-term pollution risk that may remain hidden for decades or even centuries. Mitigating this risk will require sustained, long-term management strategies, underscoring the need for proactive planning to protect groundwater quality in the CGP.

In summary, the central and eastern regions of the CGP are predicted as hotspots of groundwater NO_3^- contamination risk. The conversion of croplands to orchards drives significant NO_3^- accumulation in the deep VZ, with this accumulated NO_3^- posing a threat of groundwater contamination that may manifest over decades to centuries. Beyond nutrient-related risks, this land-use transition may also exacerbate groundwater depletion by reducing groundwater recharge fluxes and increasing reliance on groundwater pumping to meet the higher irrigation demands of orchards. These shifts in recharge dynamics and NO_3^- transport pose significant threats to regional environmental security and the sustainable utilization of water resources in the cultivated loess areas of the CGP. Addressing these challenges requires two critical steps: a comprehensive understanding of the complex

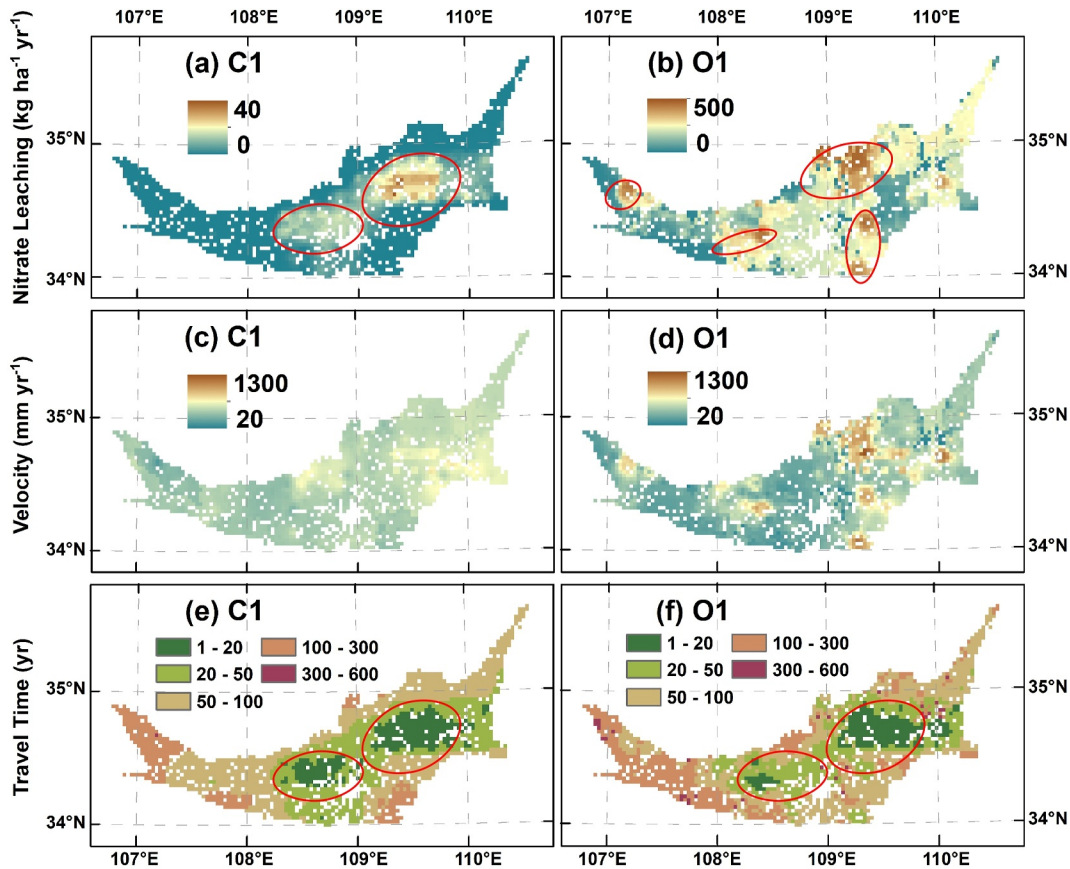

Figure 6. Distribution of NO_3^- leaching fluxes (kg ha^{-1} yr^{-1}) (a, b), velocity (mm yr^{-1}) (c, d), and travel time (yr) (e, f) for two land use scenarios based on Data set I simulations. C1, Cropland scenario; O1, Orchard scenario. Red circles indicate hotspots of groundwater NO_3^- contamination.

interactions between land use, hydrological processes, and nutrient cycling, and the implementation of targeted, long-term management strategies. Such efforts are essential to safeguard the long-term security of water resources and maintain environmental quality not only in the CGP but also in comparable agricultural regions worldwide facing similar land-use and groundwater challenges.

4. Implications for Land Use Management

This study highlights the profound impact of agricultural land-use change, specifically the conversion of croplands to orchards, on groundwater recharge and NO_3^- transport in the loess agricultural region. Fundamentally, it highlights the critical role of agricultural management practices in regulating the accumulation and migration of NO_3^- within the VZ. Notably, the issue of substantial NO_3^- accumulation in the VZ is not limited to the CGP; it has also been documented in other representative Chinese agricultural regions. These include the northeastern black soil region and the subtropical red soil region (Dong et al., 2022; Yang et al., 2024). Given the persistence of intensive farming practices (e.g., high fertilizer application, intensive irrigation) across these areas, the NO_3^- currently stored in their VZs is likely to continue leaching into groundwater over the long term. This poses enduring risks to groundwater quality, emphasizing the need for region-specific, sustainable agricultural management strategies to mitigate such threats on a broader scale.

Notably, the subtropical red soil region of China has undergone large-scale land-use transitions like those in the CGP. Since the 1990s, vast areas of forestland in this region have been converted into citrus orchards to meet agricultural production demands. A key driver of environmental risk here is the excessive N fertilization applied to these newly established orchards (practices intended to boost citrus yields), but which have likely contributed to widespread NO_3^- accumulation in the VZ. This accumulation poses a severe threat to local groundwater

security, as evidenced by previous studies (Ding et al., 2017; Gu et al., 2013; Wang et al., 2011; Yang, Wu, Song, et al., 2020, 2023). The evaluation framework developed in our study offers a critical advantage by enabling regional-scale quantification of how large-scale land-use transitions (e.g., forest-to-orchard or cropland-to-orchard conversion) impact NO_3^- accumulation and transport in the VZ. This capability supports more precise, data-driven assessments of groundwater contamination risks, avoiding the limitations of site-specific studies that cannot capture regional dynamics. Concurrently, our findings serve as an early warning for subtropical red soil regions, emphasizing the need for caution when implementing extensive land-use conversions, particularly those involving the expansion of high-fertilizer-demand orchard systems.

Globally, NO_3^- contamination of groundwater is a widespread and pressing concern (Liu et al., 2024). Recent researches have pinpointed NO_3^- pollution in groundwater linked to intensive agricultural activities across several key regions worldwide, including the Mississippi River Basin (U.S.), Rhine Basin (Europe), Yangtze and Pearl River Basins (China), and the state of Nebraska (U.S.) (Liu et al., 2024; Ray & Malakar, 2024; Van Meter et al., 2018). These findings collectively underscore the severe threats that intensive agricultural management practices pose to groundwater systems. For regions already engaged in intensive agriculture, optimizing management strategies to mitigate N loss to aquatic systems is urgent (You et al., 2024). Such strategies may include precision fertilization (matching N inputs to crop demand), improved irrigation efficiency (reducing leaching potential), or the adoption of cover crops (to retain excess N in soil). Equally critical is proactive monitoring in regions undergoing large-scale agricultural land-use and management transitions. In these areas, special attention must be paid to changes in N fertilizer inputs before and after land-use conversion. Increased fertilizer application may significantly exacerbate environmental risks, including NO_3^- leaching to groundwater. This is not only endangers groundwater quality and aquatic ecosystems but also poses risks to public health, with potentially severe economic and societal consequences.

NO_3^- leaching is not an isolated process but occurs within the broader framework of ecohydrological changes driven by deep-rooted crops like orchard trees. Beyond altering nutrient cycling, these ecohydrological shifts can trigger a cascade of interconnected soil and groundwater concerns, extending far beyond NO_3^- contamination alone. In regions with shallow groundwater tables, the introduction of orchards enhances root water uptake and reduces deep drainage, which in turn diminishes the natural leaching of salts from the root zone. Concurrently, direct groundwater extraction can further concentrate salts in the root zone by lowering the water table and drawing saline groundwater upward. Together, these processes disrupt regional water and salt balances, posing substantial risks to soil fertility and long-term agricultural productivity (Jobbágy & Jackson, 2004). Orchard establishment also contributes to other critical soil and environmental problems, including heavy metal accumulation (Liu et al., 2022), soil acidification (Jobbágy & Jackson, 2003; Wen et al., 2023), and dry soil layer formation (Li et al., 2023; Nosetto et al., 2012; Shi et al., 2020; Wang et al., 2024). Collectively, these potential impacts highlight that orchard expansion reshapes not just nutrient cycling, but also the fundamental dynamics of water and salt movement in agricultural systems. This underscores the critical need for sustainable regional agricultural management (e.g., optimized irrigation, balanced fertilization) and evidence-based policy decisions that account for the full suite of ecohydrological consequences instead of focusing solely on short-term agricultural yields. Such approaches are essential to safeguard soil health, groundwater quality, and long-term agricultural sustainability.

This study assessed the regional-scale risk of groundwater contamination induced by agricultural land-use change and identified potential hotspots. However, limited site-scale data restricted the detailed modeling of these hotspots, and more comprehensive observational data will be required to address this gap. Given the deep VZs and low recharge rates in the study area, where NO_3^- transport to groundwater can take decades to centuries, short-term fluctuations in NO_3^- movement were not evaluated. This limitation precluded an analysis of how precipitation variability affects water and NO_3^- dynamics in the VZ; future work will refine the model to specifically assess the system's response to extreme precipitation events. Additionally, variations in crop species and planting strategies significantly influence NO_3^- leaching and groundwater recharge processes. Since this analysis primarily focused on wheat-corn rotation croplands and apple orchards, the results may not capture all possible crop-management combinations across the region. Future modeling should incorporate these factors to provide a more comprehensive assessment.

5. Conclusions

Based on comprehensive soil and groundwater measurements from the CGP, a multi-column model was developed and validated to simulate water flow and NO_3^- transport in the VZ. The model showed strong agreement with observed data from deep soil profiles. Uncertainty analysis revealed that groundwater recharge and NO_3^- leaching flux estimates derived from Rosetta and global SHP data sets deviated by 3%–86% relative to values calculated using measured SHPs. Notably, SHP-related uncertainties were more pronounced in orchards than in croplands for both water and NO_3^- fluxes. Sensitivity analysis further identified soil saturation (θ_s) and the shape parameter (n) as the most influential factors. Simulations based on measured SHPs identified the central and eastern CGP as hotspots of groundwater NO_3^- contamination. Land-use transition from cropland to orchard was found to increase NO_3^- leaching fluxes by a factor of 38, reduce groundwater recharge by approximately 10%, and extend NO_3^- travel time in the VZ by about 23 years. Additionally, substantial NO_3^- accumulation in the VZ resulting from intensive fertilizer application since the 1980s is expected to continue reaching groundwater over decadal to centennial timescales. Consequently, large-scale conversion of cropland to orchard systems (especially in areas with shallow VZs and coarse-textured soils) requires careful reconsideration to minimize future groundwater contamination risks.

Conflict of Interest

The authors declare no conflicts of interest relevant to this study.

Data Availability Statement

Global SHPs data set is obtained from Gupta et al. (2020, 2022a) (https://zenodo.org/record/3935359; https://zenodo.org/record/6348799). The Rosetta program (Schaap et al., 2001) used in this study is available from the U. S. Salinity Laboratory, USDA-ARS, Riverside, California. SoilGrid250 m data set is obtained from the SoilGrids 2.0 global soil information system at 250 m resolution (SoilGrids250) developed by International Soil Reference and Information Centre (ISRIC, 2017). Land use types data set is obtained from the China Multi-Period Land Use Remote Sensing Monitoring Data set at the Resource and Environment Science and Data Center (Xu et al., 2018; https://www.resdc.cn/DOI/doi.aspx?DOIid=54). The Vadose zone thickness data were sourced from the Global Groundwater Table Distribution data set (Fan et al., 2013). Climate data are obtained from the China Meteorological Administration (CMA), National Meteorological Information Center (NMIC) (CMA, 2020; http://data.cma.cn). The original data and final data used for the analysis and figures in this study are publicly accessible (Niu & Jia, 2025; https://doi.org/10.5281/zenodo.15868041).

Acknowledgments

This study was supported by the National Natural Science Foundation of China (42225707, 42307456, and U2444217), the Strategic Priority Research Program of the Chinese Academy of Sciences (XDB40020000), the GDAS' Project of Science and Technology Development (2021GDASYL-20210102008) and the UK Natural Environment Research Council (NE/S009159/1). The authors also thank ISRIC (2017) for providing the SoilGrid250m data set, Fan et al. (2013) for providing the groundwater table depth data set, Gupta et al. (2020, 2022a) for providing the soil hydraulic parameter data sets.

References

Akbariyeh, S., Bartelt-Hunt, S., Snow, D., Li, X., Tang, Z., & Li, Y. (2018). Three-dimensional modeling of nitrate-N transport in vadose zone: Roles of soil heterogeneity and groundwater flux. *Journal of Contaminant Hydrology*, *211*, 15–25. https://doi.org/10.1016/j.jconhyd.2018.02.005

Allen, R., Pereira, L., & Smith, M. (1998). Crop evapotranspiration-Guidelines for computing crop water requirements-FAO irrigation and drainage paper 56, food and Africulture, organ of the U.N.

Ascott, M. J., Gooddy, D. C., Wang, L., Stuart, M. E., Lewis, M. A., Ward, R. S., & Binley, A. M. (2017). Global patterns of nitrate storage in the vadose zone. *Nature Communications*, *8*(1), 1416. https://doi.org/10.1038/s41467-017-01321-w

Bai, X., Shao, M. A., Jia, X. X., & Zhao, C. L. (2022). Prediction of the van Genuchten model soil hydraulic parameters for the 5-m soil profile in China's Loess Plateau. *Catena*, *210*, 105889. https://doi.org/10.1016/j.catena.2021.105889

Baram, S., Couvreur, V., Harter, T., Read, M., Brown, P. H., Kandelous, M., et al. (2016). Estimating nitrate leaching to groundwater from orchards: Comparing crop nitrogen excess, deep vadose zone data-driven estimates, and HYDRUS modeling. *Vadose Zone Journal*, *15*(11), 1–13. https://doi.org/10.2136/vzj2016.07.0061

Beven, K., & Germann, P. (2013). Macropores and water flow in soils revisited. *Water Resources Research*, *49*(6), 3071–3092. https://doi.org/10.1002/wrcr.20156

Bohlke, J. K. (2002). Groundwater recharge and agricultural contamination. *Hydrogeology Journal*, *10*(1), 153–179. https://doi.org/10.1007/s10040-001-0183-3

Bouwman, A. F., Boumans, L. J. M., & Batjes, N. H. (2002). Estimation of global NH_3 volatilization loss from synthetic fertilizers and animal manure applied to arable lands and grasslands. *Global Biogeochemical Cycles*, *16*(2), 1024. https://doi.org/10.1029/2000GB001389

Bowles, T. M., Atallah, S. S., Campbell, E. E., Gaudin, A. C. M., Wieder, W. R., & Grandy, A. S. (2018). Addressing agricultural nitrogen losses in a changing climate. *Nature Sustainability*, *1*(8), 399–408. https://doi.org/10.1038/s41893-018-0106-0

Cao, G. L., Scanlon, B. R., Han, D. M., & Zheng, C. M. (2016). Impacts of thickening unsaturated zone on groundwater recharge in the North China Plain. *Journal of Hydrology*, *537*, 260–270. https://doi.org/10.1016/j.jhydrol.2016.03.049

China Meteorological AdministrationNational Meteorological Information Center. (2020). China daily meteorological station data [Dataset]. *CMA National Data Center*. Retrieved from http://data.cma.cn

Ding, H., Zheng, X. Z., Zhang, Y. S., Zhang, J., & Chen, D. L. (2017). Gaseous losses of fertilizer nitrogen from a citrus orchard in the red soil hilly region of southeast China. *Soil Science & Plant Nutrition*, *63*(5), 419–425. https://doi.org/10.1080/00380768.2017.1381572

Dong, Y., Yang, J. L., Zhao, X. R., Yang, S. H., Mulder, J., Dörsch, P., & Zhang, G. L. (2022). Nitrate leaching and n accumulation in a typical subtropical red soil with n fertilization. *Geoderma*, *407*, 115559. https://doi.org/10.1016/j.geoderma.2021.115559

Fan, Y., Li, H., & Miguez-Macho, G. (2013). Global patterns of groundwater table depth [Dataset]. *Science*, *339*(6122), 940–943. https://doi.org/10.1126/science.1229881

Fan, Z., Wang, J., Lv, D., Li, S., Miao, Y., Hu, M., et al. (2024). Effects of cropland-to-orchard conversion on soil multifunctionality, particularly nitrogen cycling in the eastern Loess Plateau. *Frontiers in Microbiology*, *15*, 1664. https://doi.org/10.3389/fmicb.2024.1471329

Fatichi, S., Or, D., Walko, R., Vereecken, H., Young, M. H., Ghezzehei, T. A., et al. (2020). Soil structure is an important omission in Earth system models. *Nature Communications*, *11*(1), 522. https://doi.org/10.1038/s41467-020-14411-z

Feddes, R. A., Kowalik, P. J., & Zaradny, H. (1978). *Simulation of field water use and crop yield*. Centre for Agricultural Publishing and Documentation. Wageningen.

Fu, G., Crosbie, R. S., Barron, O., Charles, S. P., Dawes, W., Shi, X., et al. (2019). Attributing variations of temporal and spatial groundwater recharge: A statistical analysis of climatic and non-climatic factors. *Journal of Hydrology*, *568*, 816–834. https://doi.org/10.1016/j.jhydrol.2018.11.022

Gao, J., Lu, Y., Chen, Z., Wang, L., & Zhou, J. (2019). Land-use change from cropland to orchard leads to high nitrate accumulation in the soils of a small catchment. *Land Degradation & Development*, *30*(17), 2150–2161. https://doi.org/10.1002/ldr.3412

Gao, J., Wang, S., Li, Z., Wang, L., Chen, Z., & Zhou, J. (2021a). High nitrate accumulation in the vadose zone after land-use change from croplands to orchards. *Environmental Science & Technology*, *55*(9), 5782–5790. https://doi.org/10.1021/acs.est.0c06730

Gao, Y., Sun, X., Lu, S., & Zhang, B. (2021b). Spatio-temporal differentiation and non-point source pollution environmental risk assessment of fertilization in Shaanxi. *Journal of Northwest A & F University. Natural Science Edition*, 4976–8396. https://doi.org/10.13207/j.cnki.jnwafu.2021.02.011

Gates, J. B., Scanlon, B. R., Mu, X., & Zhang, L. (2011). Impacts of soil conservation on groundwater recharge in the semi-arid Loess Plateau, China. *Hydrogeology Journal*, *19*(4), 865–875. https://doi.org/10.1007/s10040-011-0716-3

Green, C. T., Fisher, L. H., & Bekins, B. A. (2008). Nitrogen fluxes through unsaturated zones in five agricultural settings across the United States. *Journal of Environmental Quality*, *37*(3), 1073–1085. https://doi.org/10.2134/jeq2007.0010

Gu, B., Ge, Y., Chang, S. X., Luo, W., & Chang, J. (2013). Nitrate in groundwater of China: Sources and driving forces. *Global Environmental Change*, *23*(5), 1112–1121. https://doi.org/10.1016/j.gloenvcha.2013.05.004

Gupta, S., Lehmann, P., Bonetti, S., Papritz, A., & Or, D. (2020). Global soil saturated hydraulic conductivity map using random forest in a Covariate-Based GeoTransfer Functions (CoGTF) framework at 1 km resolution [Dataset]. *Zenodo*. https://doi.org/10.5281/zenodo.3935359

Gupta, S., Lehmann, P., Bonetti, S., Papritz, A., & Or, D. (2021). Global prediction of soil saturated hydraulic conductivity using random forest in a Covariate-Based Geotransfer Function (CoGTF) framework. *Journal of Advances in Modeling Earth Systems*, *13*(4), e2020MS002242. https://doi.org/10.1029/2020MS002242

Gupta, S., Papritz, A., Lehmann, P., Hengl, T., Bonetti, S., & Or, D. (2022a). Global maps of soil water characteristics parameters developed using the random forest in a Covariate-based GeoTransfer Functions (CoGTF) framework at 1 km resolution [Dataset]. *Zenodo*. https://doi.org/10.5281/zenodo.6348799

Gupta, S., Papritz, A., Lehmann, P., Hengl, T., Bonetti, S., & Or, D. (2022b). Global mapping of soil water characteristics parameters—fusing curated data with machine learning and environmental covariates. *Remote Sensing*, *14*(8), 1947. https://doi.org/10.3390/rs14081947

Hu, W., Wang, Y. Q., Li, H. J., Huang, M. B., Hou, M. T., Li, Z., et al. (2019). Dominant role of climate in determining spatio-temporal distribution of potential groundwater recharge at a regional scale. *Journal of Hydrology*, *578*, 124042. https://doi.org/10.1016/j.jhydrol.2019.124042

Huan, H., Hu, L., Yang, Y., Jia, Y., Lian, X., Ma, X., et al. (2020). Groundwater nitrate pollution risk assessment of the groundwater source field based on the integrated numerical simulations in the unsaturated zone and saturated aquifer. *Environment International*, *137*, 105532. https://doi.org/10.1016/j.envint.2020.105532

Huang, M., Gallichand, J., & Zhong, L. (2004). Water–yield relationships and optimal water management for winter wheat in the Loess Plateau of China. *Irrigation Science*, *23*(2), 47–54. https://doi.org/10.1007/s00271-004-0092-z

Huang, T., & Pang, Z. (2011). Estimating groundwater recharge following land-use change using chloride mass balance of soil profiles: A case study at Guyuan and Xifeng in the Loess Plateau of China. *Hydrogeology Journal*, *19*(1), 177–186. https://doi.org/10.1007/s10040-010-0643-8

Huang, T., Pang, Z., & Yuan, L. (2013). Nitrate in groundwater and the unsaturated zone in (semi) arid northern China: Baseline and factors controlling its transport and fate. *Environmental Earth Sciences*, *70*(1), 145–156. https://doi.org/10.1007/s12665-012-2111-3

Huang, Y., Chang, Q., & Li, Z. (2018). Land use change impacts on the amount and quality of recharge water in the loess tablelands of China. *Science of the Total Environment*, *628–629*, 443–452. https://doi.org/10.1016/j.scitotenv.2018.02.076

Huang, Y., Li, B., & Li, Z. (2021). Conversion of degraded farmlands to orchards decreases groundwater recharge rates and nitrate gains in the thick loess deposits. *Agriculture, Ecosystems & Environment*, *314*, 107410. https://doi.org/10.1016/j.agee.2021.107410

ISRIC. (2017). SoilGrids250m: Global gridded soil information [Dataset]. *GitHub repository*. Retrieved from https://github.com/ISRICWorldSoil/SoilGrids250m

Jarvis, N. J. (2020). A review of non-equilibrium water flow and solute transport in soil macropores: Principles, controlling factors and consequences for water quality. *European Journal of Soil Science*, *71*(3), 279–302. https://doi.org/10.1111/ejss.12973

Ji, W., Huang, Y., Qian, X., Bai, E., Smith, C. K., & Li, Z. (2022). Conversion from farmland to orchards has minor effects on nitrogen biological processes in deep loess deposits. *Agriculture, Ecosystems & Environment*, *338*, 108111. https://doi.org/10.1016/j.agee.2022.108111

Jia, X. X., Shao, M. A., Zhu, Y. J., & Luo, Y. (2017). Soil moisture decline due to afforestation across the Loess Plateau, China. *Journal of Hydrology*, *546*, 113–122. https://doi.org/10.1016/j.jhydrol.2017.01.011

Jia, X. X., Zhu, P., Wei, X. R., Zhu, Y. J., Huang, M. B., Hu, W., et al. (2024). Bringing ancient loess critical zones into a new era of sustainable development goals. *Earth-Science Reviews*, *255*, 104852. https://doi.org/10.1016/j.earscirev.2024.104852

Jobbágy, E. G., & Jackson, R. B. (2003). Patterns and mechanisms of soil acidification in the conversion of grasslands to forests. *Biogeochemistry*, *64*(2), 205–229. https://doi.org/10.1023/A:1024985629259

Jobbágy, E. G., & Jackson, R. B. (2004). Groundwater use and salinization with grassland afforestation. *Global Change Biology*, *10*(8), 1299–1312. https://doi.org/10.1111/j.1365-2486.2004.00806.x

Kang, S., Gu, B., Du, T., & Zhang, J. (2003). Crop coefficient and ratio of transpiration to evapotranspiration of winter wheat and maize in a semi-humid region. *Agricultural Water Management*, *59*(3), 239–254. https://doi.org/10.1016/S0378-3774(02)00150-6

Kang, S., Hao, X., Du, T., Tong, L., Su, X., Lu, H., et al. (2017). Improving agricultural water productivity to ensure food security in China under changing environment: From research to practice. *Agricultural Water Management*, *179*, 5–17. https://doi.org/10.1016/j.agwat.2016.05.007

Klute, A., & Dirksen, C. (1986). Hydraulic conductivity of saturated soils: Field methods. *Methods Soil Analysis*, 694–700. https://doi.org/10.2136/sssabookser5.1.2ed.c29

Lawrence, D. M., Fisher, R. A., Koven, C. D., Oleson, K. W., Swenson, S. C., Bonan, G., et al. (2019). The community land model version 5: Description of new features, benchmarking, and impact of forcing uncertainty. *Journal of Advances in Modeling Earth Systems*, *11*(12), 4245–4287. https://doi.org/10.1029/2018MS001583

Li, D., Gao, G. Y., Shao, M. A., & Fu, B. J. (2016). Predicting available water of soil from particle-size distribution and bulk density in an oasis-desert transect in northwestern China. *Journal of Hydrology*, *538*, 539–550. https://doi.org/10.1016/j.jhydrol.2016.04.046

Li, H., Si, B. C., & Li, M. (2018). Rooting depth controls potential groundwater recharge on hillslopes. *Journal of Hydrology*, *564*, 164–174. https://doi.org/10.1016/j.jhydrol.2018.07.002

Li, H., Si, B. C., Ma, X., & Wu, P. (2019). Deep soil water extraction by apple sequesters organic carbon via root biomass rather than altering soil organic carbon content. *Science of the Total Environment*, *670*, 662–671. https://doi.org/10.1016/j.scitotenv.2019.03.267

Li, H. J., Li, H., Wu, Q. F., Si, B. C., Jobbágy, E. G., & McDonnell, J. J. (2023). Afforestation triggers water mining and a single pulse of water for carbon trade-off in deep soil. *Agriculture, Ecosystems & Environment*, *356*, 108655. https://doi.org/10.1016/j.agee.2023.108655

Li, Z., Chen, X., Liu, W., & Si, B. C. (2017). Determination of groundwater recharge mechanism in the deep Loessial unsaturated zone by environmental tracers. *Science of the Total Environment*, *586*, 827–835. https://doi.org/10.1016/j.scitotenv.2017.02.061

Li, Z., Guo, S. L., Zhang, F., & Zou, J. L. (2011). Effects of apple orchard converted from cropland on C and N storages in terrestrial system of slopping cultivated land in the Loess Gully regions. *Journal of Plant Nutrition and Fertilizers*, *17*(4), 919–924. https://doi.org/10.11674/zwyf.2011.0510

Liao, L., Green, C. T., Bekins, B. A., & Böhlke, J. K. (2012). Factors controlling nitrate fluxes in groundwater in agricultural areas. *Water Resources Research*, *48*(6). https://doi.org/10.1029/2011WR011008

Lide, D. R. (2002). CRC handbook of chemistry and physics (83rd ed.).

Liu, C., Du, T., Li, F., Kang, S., Li, S., & Tong, L. (2012). Trunk sap flow characteristics during two growth stages of apple tree and its relationships with affecting factors in an arid region of northwest China. *Agricultural Water Management*, *104*, 193–202. https://doi.org/10.1016/j.agwat.2011.12.014

Liu, X., Beusen, A. H. W., van Grinsven, H. J. M., Wang, J., van Hoek, W. J., Ran, X., et al. (2024). Impact of groundwater nitrogen legacy on water quality. *Nature Sustainability*, *7*(7), 891–900. https://doi.org/10.1038/s41893-024-01369-9

Liu, Y. L., Liu, S. L., Wu, M., Tian, X. L., & Liu, S. Y. (2022). Effect of land use/land cover change on the concentration of Se and heavy metals in soils from a "return cropland to forest" area, southwest China. *Environmental Sciences*, *43*(6), 3262–3268. (in Chinese). https://doi.org/10.13227/j.hjkx.202109035

Lu, S., Meng, P., Zhang, J. S., Yin, C. J., & Sun, S. Y. (2015). Changes in soil organic carbon and total nitrogen in croplands converted to walnut-based agroforestry systems and orchards in southeastern Loess Plateau of China. *Environmental Monitoring and Assessment*, *187*(11), 688. https://doi.org/10.1007/s10661-014-4131-9

Lu, Y., Chen, Z., Kang, T., Zhang, X., Bellarby, J., & Zhou, J. (2016). Land-use changes from arable crop to kiwi-orchard increased nutrient surpluses and accumulation in soils. *Agriculture, Ecosystems & Environment*, *223*, 270–277. https://doi.org/10.1016/j.agee.2016.03.019

Lyu, S., Chen, W., Wen, X., & Chang, A. C. (2019). Integration of HYDRUS-1D and MODFLOW for evaluating the dynamics of salts and nitrogen in groundwater under long-term reclaimed water irrigation. *Irrigation Science*, *37*(1), 35–47. https://doi.org/10.1007/s00271-018-0600-1

Ma, H., Yang, D., Lei, H., Cai, J., & Kusuda, T. (2011). Application and improvement of Hydrus-1D model for analyzing water cycle in an agricultural field. *Transactions of the Chinese Society of Agricultural Engineering*, *27*(3), 6–12. https://doi.org/10.3969/J.ISSN.1002-6819.2011.3.002

Maharjan, B., Venterea, R. T., & Rosen, C. (2014). Fertilizer and irrigation management effects on nitrous oxide emissions and nitrate leaching. *Agronomy Journal*, *106*(2), 703–714. https://doi.org/10.2134/agronj2013.0179

Mahvi, A. H., Nouri, J., Babaei, A. A., & Nabizadeh, R. (2005). Agricultural activities impact on groundwater nitrate pollution. *International journal of Environmental Science and Technology*, *2*(1), 41–47. https://doi.org/10.1007/BF03325856

Millington, R. J., & Quirk, J. M. (1961). Permeability of porous solids. *Transactions of the Faraday Society*, *57*, 1200–1207. https://doi.org/10.1039/TF9615701200

Min, L., Shen, Y., Pei, H., & Wang, P. (2018). Water movement and solute transport in deep vadose zone under four irrigated agricultural land-use types in the North China Plain. *Journal of Hydrology*, *559*, 510–522. https://doi.org/10.1016/j.jhydrol.2018.02.037

Mohajerani, H., Teschemacher, S., & Casper, M. C. (2021). A comparative investigation of various pedotransfer functions and their impact on hydrological simulations. *Water*, *13*(10), 22. https://doi.org/10.3390/w13101401

Niu, L. T., & Jia, X. X. (2025). Orchard expansion may diminish groundwater replenishment while amplifying nitrate pollution in a cultivated loess critical zone [Dataset]. *Zenodo*. https://doi.org/10.5281/zenodo.15868041

Niu, X. Q., Jia, X. X., Yang, X. F., Wang, J., Wei, X. R., Wu, L. H., & Shao, M. A. (2022). Tracing the sources and fate of NO_3^- in the vadose zone–groundwater system of a thousand-year-cultivated region. *Environmental Science & Technology*, *56*(13), 9335–9345. https://doi.org/10.1021/acs.est.1c06289

Niu, X. Q., Liu, C. G., Jia, X. X., & Zhu, J. (2021). Changing soil organic carbon with land use and management practices in a thousand-year cultivation region. *Agriculture, Ecosystems & Environment*, *322*, 107639. https://doi.org/10.1016/j.agee.2021.107639

Nosetto, M. D., Jobbágy, E. G., Brizuela, A. B., & Jackson, R. B. (2012). The hydrologic consequences of land cover change in central Argentina. *Agriculture, Ecosystems & Environment*, *154*, 2–11. https://doi.org/10.1016/j.agee.2011.01.008

Padilla, F. M., Gallardo, M., & Manzano-Agugliaro, F. (2018). Global trends in nitrate leaching research in the 1960–2017 period. *Science of the Total Environment*, *643*, 400–413. https://doi.org/10.1016/j.scitotenv.2018.06.215

Paschalis, A., Bonetti, S., Guo, Y., & Fatichi, S. (2022). On the uncertainty induced by pedotransfer functions in terrestrial biosphere modeling. *Water Resources Research*, *58*(9), e2021WR031871. https://doi.org/10.1029/2021WR031871

Qiao, J. B., Zhu, Y. J., Jia, X. X., Huang, L. M., & Shao, M. A. (2018). Development of pedotransfer functions for soil hydraulic properties in the critical zone on the Loess Plateau, China. *Hydrological Processes*, *32*(18), 2915–2921. https://doi.org/10.1002/hyp.13216

Raats, P. A. C. (1974). Steady flows of water and salt in uniform soil profiles with plant roots. *Soil Science Society of America Journal*, *38*(5), 717–722. https://doi.org/10.2136/sssaj1974.03615995003800050012x

Rao, E., & Puttanna, K. (2000). Nitrates, agriculture and environment. *Current Science*, *79*(9), 1163–1168. http://www.jstor.org/stable/24105267

Ray, C., & Malakar, A. (2024). Nitrate contamination in Nebraska's Ogallala aquifer. *Science*, *386*(6719), 280. https://doi.org/10.1126/science.adr3796

Robertson, W. M., Bohlke, J. K., & Sharp, J. M., Jr. (2017). Response of deep groundwater to land use change in desert basins of the trans-Pecos region, Texas, USA: Effects on infiltration, recharge, and nitrogen fluxes. *Hydrological Processes*, *31*(13), 2349–2364. https://doi.org/10.1002/hyp.11178

Schaap, M. G., Leij, F. J., & van Genuchten, M. T. (2001). ROSETTA: A computer program for estimating soil hydraulic parameters with hierarchical pedotransfer functions [Software]. *Journal of Hydrology*, *251*(3–4), 163–176. https://doi.org/10.1016/s0022-1694(01)00466-8

Shen, H., Xu, F., Zhao, R., Xing, X., & Ma, X. (2020). Optimization of sowing date, irrigation, and nitrogen management of summer maize using the DSSAT-CERES-Maize model in the Guanzhong plain, China. *Transactions of the ASABE*, *63*(4), 789–797. https://doi.org/10.13031/trans.13654

Shi, D. P., Tan, H. B., Rao, W. B., Liu, Z. H., & Elenga, H. I. (2020). Variations in water content of soil in apricot orchards in the western hilly regions of the Chinese Loess Plateau. *Vadose Zone Journal*, *19*(1), e20034. https://doi.org/10.1002/vzj2.20034

Šimůnek, J. J., Saito, H., Sakai, M., & van Genuchten, M. T. (2008). *The HYDRUS-1D software package for simulating the one-dimensional movement of water, heat, and multiple solutes in variably-saturated media, version 4.0*. HYDRUS Software Series 3, Department of Environmental Sciences, University of California Riverside, 315.

SPWRD (Shaanxi Provincial Department of Water Resources). (2018). *Shaanxi water resources bulletin*. China Statistics Press. Retrieved from https://slt.shaanxi.gov.cn/zfxxgk/fdzdgknr/zdgz/szygb/201909/t20190902_1761083.html

Suchy, M., Wassenaar, L. I., Graham, G., & Zebarth, B. (2018). High-frequency NO_3^- isotope ($\delta^{15}N$, $\delta^{18}O$) patterns in groundwater recharge reveal that short-term changes in land use and precipitation influence nitrate contamination trends. *Hydrology and Earth System Sciences*, *22*(8), 4267–4279. https://doi.org/10.5194/hess-22-4267-2018

SXBS (Shaanxi Bureau of Statistics). (2021). *Shaanxi statistical yearbook 2020*. China Statistics Press. Retrieved from https://tjj.shaanxi.gov.cn/tjsj/ndsj/tjnj/sxtjnj/index.html?2021

Tian, H., Jin, M., Sohail, S., Ma, C. C., Bai, C. Y., Qiao, J. B., et al. (2024). The trade-off between soil water recovery and nitrate leaching following the orchard-to-cropland conversion in the Chinese Loess Plateau. *Scientific Reports*, *14*(1), 29781. https://doi.org/10.1038/s41598-024-80192-w

Turkeltaub, T., Ascott, M. J., Gooddy, D. C., Jia, X. X., Shao, M. A., & Binley, A. (2020). Prediction of regional-scale groundwater recharge and nitrate storage in the vadose zone: A comparison between a global model and a regional model. *Hydrological Processes*, *34*(15), 3347–3357. https://doi.org/10.1002/hyp.13834

Turkeltaub, T., Dahan, O., & Kurtzman, D. (2014). Investigation of groundwater recharge under agricultural fields using transient deep vadose zone data. *Vadose Zone Journal*, *13*(4), 1–13. https://doi.org/10.2136/vzj2013.10.0176

Turkeltaub, T., Jia, X. X., Zhu, Y. J., Shao, M. A., & Binley, A. (2018). Recharge and nitrate transport through the deep vadose zone of the Loess Plateau: A regional-scale model investigation. *Water Resources Research*, *54*(7), 4332–4346. https://doi.org/10.1029/2017WR022190

Turkeltaub, T., Jia, X. X., Zhu, Y. J., Shao, M. A., & Binley, A. (2021). A comparative study of conceptual model complexity to describe water flow and nitrate transport in deep unsaturated loess. *Water Resources Research*, *57*(8), e2020WR029250. https://doi.org/10.1029/2020WR029250

Turkeltaub, T., Kurtzman, D., Russak, E. E., & Dahan, O. (2015). Impact of switching crop type on water and solute fluxes in deep vadose zone. *Water Resources Research*, *51*(12), 9828–9842. https://doi.org/10.1002/2015WR017612

van Genuchten, M. T. (1980). A closed-form equation for predicting the hydraulic conductivity of unsaturated soils. *Soil Science Society of America Journal*, *44*(5), 892–898. https://doi.org/10.2136/sssaj1980.03615995004400050002x

Van Meter, K. J., Van Cappellen, P., & Basu, N. B. (2018). Legacy nitrogen may prevent achievement of water quality goals in the Gulf of Mexico. *Science*, *360*(6387), 427–430. https://doi.org/10.1126/science.aar4462

Vrugt, J. A., van Wijk, M. T., Hopmans, J. W., & Šimůnek, J. (2001). One-two-and three-dimensional root water uptake functions for transient modeling. *Water Resources Research*, *37*(10), 2457–2470. https://doi.org/10.1029/2000WR000027

Wang, C., Lu, H., Gu, W., Wu, N., Zhang, J., Zuo, X., et al. (2017). The spatial pattern of farming and factors influencing it during the Peiligang culture period in the middle Yellow River valley, China. *Science Bulletin*, *62*(23), 1565–1568. https://doi.org/10.1016/J.SCIB.2017.10.003

Wang, D., Li, P., Yang, N., Yang, C., Zhou, Y., & Li, J. (2023). Distribution, sources and main controlling factors of nitrate in a typical intensive agricultural region, northwestern China: Vertical profile perspectives. *Environmental Research*, *237*, 116911. https://doi.org/10.1016/j.envres.2023.116911

Wang, H., Wang, Z., & Zheng, T. (2018a). Study on the present situation of groundwater resources and the networking of monitoring stations in Shaanxi Province. *Groundwater Series*, *40*(5), 44–49. (in Chinese).

Wang, S. Q., Wei, S. C., Liang, H. Y., Zheng, W. B., Li, X. X., Hu, C. S., et al. (2019). Nitrogen stock and leaching rates in a thick vadose zone below areas of long-term nitrogen fertilizer application in the North China plain: A future groundwater quality threat. *Journal of Hydrology*, *576*, 28–40. https://doi.org/10.1016/j.jhydrol.2019.06.012

Wang, W., Wang, Y., Sun, Q., Zhang, M., Qiang, Y., & Liu, M. (2018b). Spatial variation of saturated hydraulic conductivity of a loess slope in the south Jingyang Plateau, China. *Engineering Geology*, *236*, 70–78. https://doi.org/10.1016/j.enggeo.2017.08.002

Wang, X., Fan, Y. L., Yan, M. F., Tao, Z., He, D., Du, G. Y., et al. (2024). Direct characterization of deep soil water depletion reveals hydraulic adjustment of apple trees to edaphic changes. *Agricultural and Forest Meteorology*, *348*, 109932. https://doi.org/10.1016/j.agrformet.2024.109932

Wang, X., Feng, W., Wang, W. K., Cao, Y. Q., & Xia, Y. B. (2015a). Migrating and transforming rule of nitrogen in unsaturated zone in Guanzhong basin based on HYDRUS-1D mode. *North China Geology*, *38*, 291–298. https://doi.org/10.3969/j.issn.1672-4135.2015.04.008

Wang, X. Y. (2014). *Study on characteristics of the temporal and spatial variation of nutrient resource utilization in Shaanxi Province*. (Doctoral Dissertation). Northwest A&F University.

Wang, Y., Shao, M. A., Han, X., & Liu, Z. (2015b). Spatial variability of soil parameters of the Van Genuchten model at a regional scale. *CLEAN – Soil, Air, Water*, *43*(2), 271–278. https://doi.org/10.1002/clen.201300903

Wang, Y., Zhang, B., Lin, L., & Zepp, H. (2011). Agroforestry system reduces subsurface lateral flow and nitrate loss in Jiangxi province, China. *Agriculture, Ecosystems & Environment*, *140*(3), 441–453. https://doi.org/10.1016/j.agee.2011.01.007

Weihermüller, L., Lehmann, P., Herbst, M., Rahmati, M., Verhoef, A., Or, D., et al. (2021). Choice of pedotransfer functions matters when simulating soil water balance fluxes. *Journal of Advances in Modeling Earth Systems*, *13*(3), 30. https://doi.org/10.1029/2020MS002404

Wen, H. Y., Wu, H. Y., Dong, Y., Feng, W. J., Lu, Y., Hu, Y. M., & Zhang, G. L. (2023). Differential soil acidification caused by parent materials and land-use changes in the Pearl River Delta region. *Soil Use & Management*, *39*(1), 329–341. https://doi.org/10.1111/sum.12867

Wu, H., Dong, Y., Gao, L., Song, X., Liu, F., Peng, X., & Zhang, G. L. (2021). Identifying nitrate sources in surface water, regolith and groundwater in a subtropical red soil critical zone by using dual nitrate isotopes. *Catena*, *198*, 104994. https://doi.org/10.1016/j.catena.2020.104994

Xia, Y. (2008). *The process modeling of soil water carrying capacity for vegetation in small watershed within the wind-water crisscrossed erosion zone on the Loess Plateau*. (Doctoral Dissertation). Institute of Geographic Sciences and Natural Resources Research, CAS.

Xu, X. L., Liu, J. Y., Zhang, S. W., Li, R. D., Yan, C. Z., & Wu, S. X. (2018). China multi-period land use remote sensing monitoring dataset [Dataset]. *Resource and Environment Science and Data Center*. https://doi.org/10.12078/2018070201

Xue, D., Botte, J., Baets, B., DeAccoe, F., Nestler, A., Taylor, P., et al. (2009). Present limitations and future prospects of stable isotope methods for nitrate source identification in surface- and groundwater. *Water Research*, *43*(5), 1159–1170. https://doi.org/10.1016/j.watres.2008.12.048

Yang, S. H., Dong, Y., Song, M., Gu, J., Shi, Y., Wu, H., et al. (2024). Deep nitrate accumulation in typical black soil critical zones of northeast China. *Science of the Total Environment*, *953*, 176050. https://doi.org/10.1016/j.scitotenv.2024.176050

Yang, S. H., Dong, Y., Wu, H., Song, X., Zhao, X., Yang, J., & Zhang, G. L. (2023). Deep accumulation of soluble organic nitrogen after land-use conversion from woodlands to orchards in a subtropical hilly region. *Science of the Total Environment*, *863*, 160931. https://doi.org/10.1016/j.scitotenv.2022.160931

Yang, S. H., Wu, H. Y., Dong, Y., Zhao, X. R., Song, X. D., Yang, J. L., et al. (2020). Deep nitrate accumulation in a highly weathered subtropical critical zone depends on the regolith structure and planting year. *Environmental Science & Technology*, *54*(21), 13739–13747. https://doi.org/10.1021/acs.est.0c04204

Yang, S. H., Wu, H. Y., Song, X. D., Dong, Y., Zhao, X. R., Cao, Q., et al. (2020). Variation of deep nitrate in a typical red soil critical zone: Effects of land use and slope position. *Agriculture, Ecosystems & Environment*, *297*, 106966. https://doi.org/10.1016/j.agee.2020.106966

You, L., Ros, G. H., Chen, Y., Zhang, F., & de Vries, W. (2024). Optimized agricultural management reduces global cropland nitrogen losses to air and water. *Nature Food*, *5*(12), 995–1004. https://doi.org/10.1038/s43016-024-01076-w

Zhang, C. Y., Zhang, S., Yin, M. Y., Ma, L. N., He, Z., & Ning, Z. (2013). Nitrogen isotope studies of nitrate contamination of the thick vadose zones in the wastewater-irrigated area. *Environmental Earth Sciences*, *68*(5), 1475–1483. https://doi.org/10.1007/s12665-012-1878-6

Zhang, M., Lu, Y., Heitman, J., Horton, R., & Ren, T. (2017). Temporal changes of soil water retention behavior as affected by wetting and drying following tillage. *Soil Science Society of America Journal*, *81*(6), 1288–1295. https://doi.org/10.2136/sssaj2017.01.0038

Zhang, P. X. (2018). *Study on the change characteristic and monitoring assessment of ground water in Guanzhong plain of Shaanxi province* (Master Dissertation). Xi'an University of Technology.

Zhang, W. L., Tian, Z. X., Zhang, N., & Li, X. Q. (1996). Nitrate pollution of groundwater in northern China. *Agriculture, Ecosystems & Environment*, *59*(3), 223–231. https://doi.org/10.1016/0167-8809(96)01052-3

Zhang, Y., Schaap, M. G., & Zha, Y. (2018a). A high-resolution global map of soil hydraulic properties produced by a hierarchical parameterization of a physically based water retention model. *Water Resources Research*, *54*(12), 9774–9790. https://doi.org/10.1029/2018wr023539

Zhang, Z. Q., Li, M., Si, B. C., & Feng, H. (2018b). Deep rooted apple tress decrease groundwater recharge in the highland region of the Loess Plateau, China. *Science of the Total Environment*, *622–623*, 584–593. https://doi.org/10.1016/j.scitotenv.2017.11.230

Zhang, Z. Q., Si, B. C., Li, H. J., & Li, M. (2019). Quantify piston and preferential water flow in deep soil using Cl^- and soil water profiles in deforested apple orchards on the Loess Plateau. *China. Water*, *11*(10), 2183. https://doi.org/10.3390/w11102183

Zhao, C. L., Shao, M. A., Jia, X. X., Nasir, M., & Zhang, C. C. (2016). Using pedotransfer functions to estimate soil hydraulic conductivity in the Loess Plateau of China. *Catena*, *143*, 1–6. https://doi.org/10.1016/j.catena.2016.03.037

Zhao, H., Lakshmanan, P., Wang, X., Xiong, H., Yang, L., Liu, B., et al. (2022). Global reactive nitrogen loss in orchard systems: A review. *Science of the Total Environment*, *821*, 153462. https://doi.org/10.1016/j.scitotenv.2022.153462

Zhao, J., Yuan, X., Liu, Z., Shi, H., Zhai, B., & Zhu, Y. (2024). Divergent responses of soil physicochemical properties in 6-m profiles to long-term overfertilization in rainfed apple orchards on China's Loess Plateau. *Agriculture, Ecosystems & Environment*, *361*, 108817. https://doi.org/10.1016/j.agee.2023.108817

Zhao, Z. P., Yan, S., Liu, F., Wang, X. Y., & Tong, Y. (2014). Analysis of nitrogen inputs and soil nitrogen loading in different kinds of orchards in Shaanxi province. *Acta Ecologica Sinica*, *34*(19), 5642–5649. https://doi.org/10.5846/STXB201301120087

Zhu, X., Miao, P., Qin, J., Li, W., Wang, L., Chen, Z., & Zhou, J. (2023). Spatiotemporal variations of nitrate pollution of groundwater in the intensive agricultural region: Hotspots and driving forces. *Journal of Hydrology*, *623*, 129864. https://doi.org/10.1016/j.jhydrol.2023.129864

References From the Supporting Information

BJBS (Baoji Bureau of Statistics). (2023). *Baoji statistical yearbook 2022*. China Statistics Press. Retrieved from http://tjj.baoji.gov.cn/col1925/col18051/202401/P020241228300878571173.pdf

Hengl, T., Mendes de Jesus, J., Heuvelink, G. B. M., Ruiperez Gonzalez, M., Kilibarda, M., Blagotić, A., et al. (2017). SoilGrids250m: Global gridded soil information based on machine learning. *PLoS One*, *12*(2), e0169748. https://doi.org/10.1371/journal.pone.0169748

WNBS (Weinan Bureau of Statistics). (2023). *Weinan statistical Yearbook 2022*. China Statistics Press. Retrieved from https://tjj.weinan.gov.cn/tjsju/tjnj/1739179184143626241.html

XABS (Xi'an Bureau of Statistics). (2023). *Xi'an statistical yearbook 2022*. China Statistics Press. Retrieved from https://tjj.xa.gov.cn/tjnj/2023/zk/indexch.htm

XYBS (Xianyang Bureau of Statistics). (2023). *Xianyang statistical yearbook 2022*. China Statistics Press. Retrieved from https://tjj.xianyang.gov.cn/sjzx/xysj/202403/P020240410411862312181.pdf